SENSITIVITY OF THE PLUME RISE MODEL IN THE ESTIMATION OF BIOMASS BURNING PLUME INJECTION HEIGHTS IN SOUTH AMERICA

Gonzalo Andrés Guajardo Ferrada

Master's Dissertation of the Graduate Course in Meteorology, guided by Dr. Saulo Ribeiro de Freitas, approved in july 14, 2016.

URL of the original document:
<http://urlib.net/8JMKD3MGP3W34P/3M2LFGB>

INPE

São José dos Campos

2016

SENSITIVITY OF THE PLUME RISE MODEL IN THE ESTIMATION OF BIOMASS BURNING PLUME INJECTION HEIGHTS IN SOUTH AMERICA

Gonzalo Andrés Guajardo Ferrada

Master's Dissertation of the Graduate Course in Meteorology, guided by Dr. Saulo Ribeiro de Freitas, approved in july 14, 2016.

URL of the original document:
<http://urlib.net/8JMKD3MGP3W34P/3M2LFGB>

INPE

São José dos Campos

2016

Aluno (a): *Gonzalo Andrés Guajardo Ferrada*

Título: "SENSITIVITY OF THE PLUME RISE MODEL IN THE ESTIMATION OF BIOMASS BURNING PLUME INJECTION HEIGHTS IN SOUTH AMERICA"

Aprovado (a) pela Banca Examinadora em cumprimento ao requisito exigido para obtenção do Título de *Mestre* em *Meteorologia*

Dr.   Nelson Jesuz Ferreira

Presidente / INPE / Cachoeira Paulista - SP

Dr.   Saulo Ribeiro de Freitas

Orientador(a) / INPE / Cachoeira Paulista - SP

Dr.   Nilton Manuel Évora do Rosário

Convidado(a) / UNIFESP / São Paulo - SP

Este trabalho foi aprovado por:

( ) maioria simples

(x) unanimidade

São José dos Campos, 14 de julho de 2016

ACKNOWLEDGMENTS

ABSTRACT

This study had the aim to evaluate the new developments on the Plume Rise Model (PRM), embedded into the BRAMS model. PRM computes the biomass burning plume injection heights and returns that information to the host model. Then, the atmospheric model releases all the fire emissions at this height. New developments are based on the initialization data used by the PRM, using fire size and fire radiative power (FRP) from remote sensing. The main difference between the two new versions is the conversion parameter (β) used to convert from FRP to the plume convective flux. In addition, a new scheme to generate daily fire emission fluxes is implemented, using the fire radiative energy (computed from remote sensing) in the Brazilian Biomass Burning Emission Model (3BEM-FRE). Model results using the three versions of the PRM are compared with observed airborne CO and O_3 data from the South American Biomass Burning Analysis (SAMBBA) campaign, which took place in southern Amazonia and *Cerrado* regions in September 2012. Results show that improvements in both 3BEM-FRE and PRM models, have a better performance in the vertical and horizontal reproduction of CO and O_3 than the original versions of both models, especially in the middle and upper troposphere, specially, reproducing fires over the *Cerrado* region. Nevertheless, new versions of both models have some difficulty to reproduce the emissions by the end of the campaign, probably due to the cumulus parameterization used, which overestimated the precipitation in the region of study.]

Keywords: Biomass burning, numerical modeling, fire emissions.

SENSIBILIDADE DO MODELO PLUME RISE MODEL NA ESTIMATIVA DA ALTURA DE INJEÇÃO DE PLUMAS DE QUEIMADAS NA AMÉRICA DO SUL

RESUMO

Este estudo teve como objetivo avaliar os novos desenvolvimentos no modelo Plume Rise Model (PRM), inserido no modelo BRAMS. O modelo PRM calcula a altura de injeção das plumas das queimadas e devolve esse dado para o modelo atmosférico. Logo, o modelo BRAMS libera todas as emissões das queimadas nesta altura. Os novos desenvolvimentos, baseiam-se no uso da área do fogo e a potência radiativa do fogo (FRP), obtidos via sensoriamento remoto, que são usados para a inicialização do PRM. A diferença entre as duas novas versões está no parâmetro de conversão de FRP para o fluxo conectivo das plumas (β). Também, é implementado um esquema para gerar as emissões das queimadas no modelo 3BEM que usa a energia radiativa do fogo (calculada a partir da FRP) para estimar a emissões diárias dos fogos detectados (3BEM-FRE). Os resultados das simulações com as novas versões do PRM são comparados com dados de voos da campanha South American Biomass Burning Analysis (SAMBBA), que teve lugar no sul da Amazônia e Cerrado brasileiro em setembro de 2012. Os resultados mostram que os desenvolvimentos feitos no 3BEM-FRE e no PRM, tiveram melhor desempenho na reprodução vertical e horizontal do CO e O_3 emitido pelas queimadas, do que as versões originais destes modelos, especialmente na troposfera média e alta. Embora, haja dificuldade para reproduzir as emissões para o final da campanha, provávelmente devido à parametrização de cumulus utilizada, que superestimou a precipitação na região de estudo.

Palavras chave: queimadas, modelagem numérica, emissões.

x

LIST OF FIGURES

LIST OF TABLES

CONTENTS

1   INTRODUCTION

Biomass burning is the combustion of organic matter. It may be caused by natural or anthropogenic sources. During the combustion process, great amounts of aerosols (predominantly, carbon particles) and gases (e.g., carbon monoxide, nitrous oxides, etc.) are released into the atmosphere, including greenhouse gases (water vapor, carbon dioxide, methane, among others) and ozone precursors. In South America, biomass burning occurs mainly between July and October over Southern Amazon and *Cerrado* (savanna) biomes, matching with the dry season of these regions (ANDREAE, 1991). Depending on the available energy of the fire, (resulting in the convection that make the fire plume to develop) and the meteorological conditions (FROMM; SERVRANCKX, 2003), emitted particles and gases can reach heights above 10 km (Fig. 1.1; FREITAS et al., 2010; PAUGAM et al., 2015a). In addition, they can stay in the atmosphere for several days or even weeks (FREITAS et al., 2005) until they start their deposition process. Biomass burning emissions products can absorb and scatter solar radiation (REID et al., 1998), modify the clouds microphysics, albedo and their precipitation processes, due to the ability of the emitted particles can act as cloud condensation nuclei (COTTON; PIELKE, 2007; ROSENFELD, 1999). In numerical modeling of the environment, an essential feature of physical processes associated to biomass burning emissions, is the estimation of the fire plume injection height, produced during the flaming phase (FREITAS et al., 2006). This is due to the strong dependence of the transport and dispersion of the products embedded into the smoke plume on the vertical structure of the horizontal wind. Furthermore, a plume injection within the planetary boundary layer, or into the free troposphere, implies in a different production and removal rates of secondary gases, as the case of tropospheric ozone (FREITAS et al., 2006, 2010).

Fire plume dynamics include different spatial scales, from a few millimeters around the plume to several hundred meters when the fire plume interacts with the atmosphere, generating turbulent mixing and de/entrainment of the plume
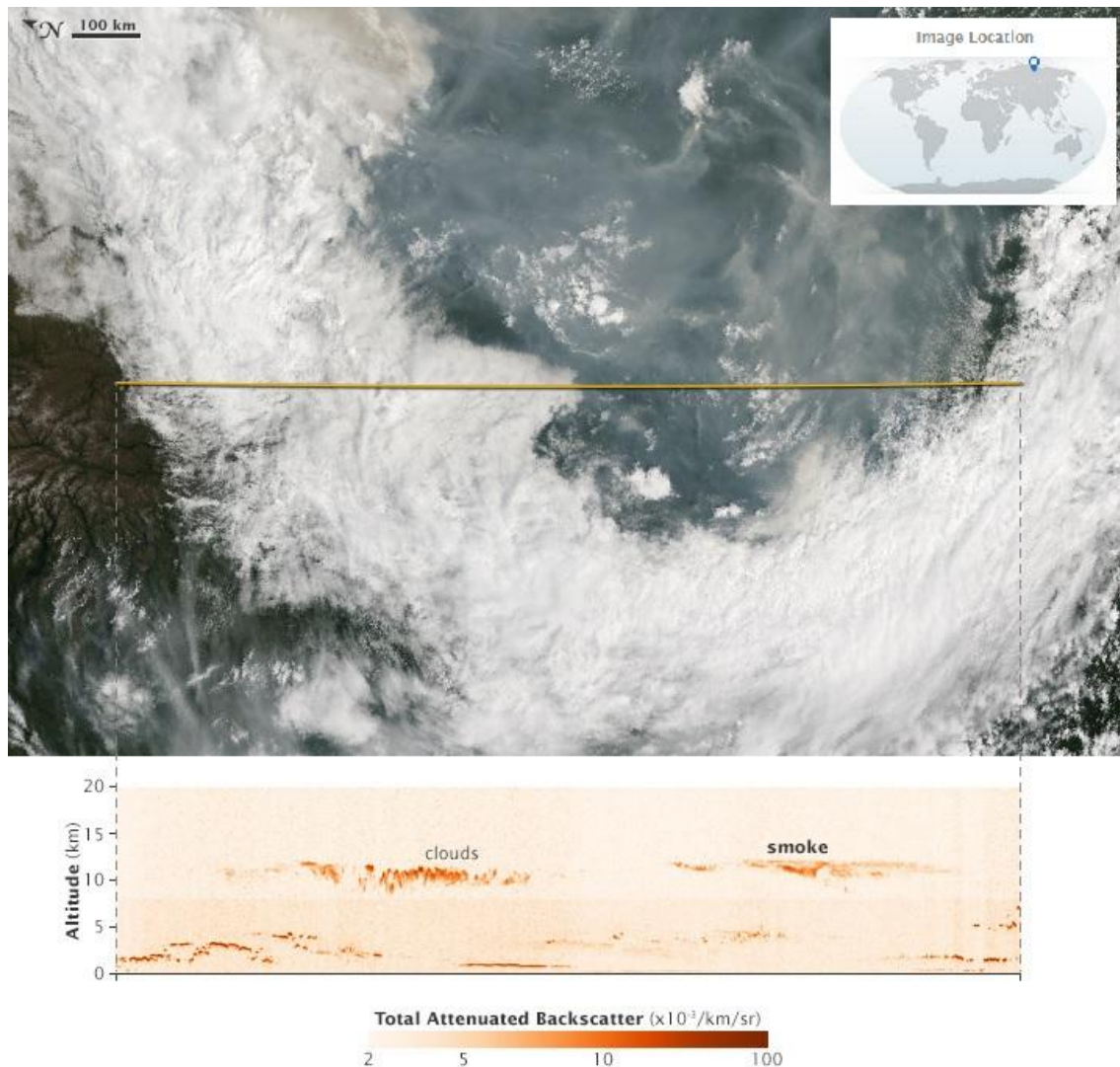
Figure 1.1 Vertical profile of total attenuated backscatter, showing the plume injection height of Siberian fires in 18 July 2014. The background (top) image was captured by MODIS Aqua satellite and provides a true-color view of the fire from directly above. The yellow line indicates the path of the CALIPSO satellite and its laser light (LIDAR). The MODIS image has been rotated so that it and the line that depicts the CALIPSO flight track are aligned horizontally (Source: NASA Earth Observatory, http://earthobservatory.nasa.gov/IOTD/view.php?id=84091).

with the ambient (FREITAS et al., 2006, 2010; PAUGAM et al., 2015a). This kind of processes are not resolved explicitly by the current transport models, because they are run with a computational grid greater than 1 km in the horizontal, being necessary the use of parameterizations. For this case, the parameterization is called "injection height" (InjH), defined as the model vertical height (or layer) where fire emissions are not controlled by the plume dynamics

anymore and, therefore, they are released into the free atmosphere (COLARCO, 2004).

In chemistry transport models (CTMs), the 1-D Plume Rise Model (PRM) (FREITAS et al., 2006, 2010; LATHAM, 1994) is widely used to estimate the biomass burning plume injection heights. It simulates the sub grid vertical transport of a 3-D transport model (host) which, in turn, provides the boundary conditions to the PRM. This allows an explicit development of the smoke plume. Thus, the plume injection height computed by the PRM is used in the emission source field of the host model to define the effective injection height, releasing all the flaming phase emissions in this height or layer (FREITAS et al., 2006). Recently, PRM was developed into a second (PRMv1) and third (PRMv2) version. PRMv1 include the estimation of the convective heat flux (CHF) from fire radiative power (FRP) observations via remote sensing (VAL MARTIN et al., 2012). Moreover, PRMv2 includes improvements in the dynamics of the model, with more physical constraints in terms of de/entrainment and the conservation of mass (PAUGAM et al., 2015b). PRMv2 was optimized by using fires detected in North America in 2003.

Currently, at the Center for Weather Forecast and Climate Studies (CPTEC), the environment transport model used is the Brazilian developments on the Regional Atmospheric Modelling System (BRAMS, formerly CCATT-BRAMS; (FREITAS et al., 2009, 2016; LONGO et al., 2010, 2013). It already has embedded the first version of the PRM (PRMv0), which uses CHF data from inventories to compute the plume injection height. The traditional method to estimate daily fluxes of biomass burning emissions in the Brazilian Biomass Burning Emission Model (3BEM), coupled to the BRAMS, are underestimating the pollutants, especially, in the *Cerrado* region. This is the first work that evaluates the developments on the 3BEM model made by Pereira et al. (2009), contributing to update the CPTEC product, putting the new developments of the PRM into the BRAMS modelling system. Thus, is expected to increase the accuracy of environmental forecasts for South America.

1.1. Objectives

The main objective of this study is to evaluate the vertical and horizontal distribution of biomass burning emissions computed by the 3BEM model and the second version of the Plume Rise Model (PRMv1) into the BRAMS over South America, using trace gases data from the South American Biomass Burning Analysis (SAMBBA) campaign occurred in northern-center Brazil during 2012.

The secondary or specific aims are:

- To study the performance of PRMv0, PRMv1 and PRMv2 in off-line mode, using detected fires in North America in 2003.

- To implement and test a new biomass burning emissions scheme in the Brazilian Biomass Burning Emissions Model (3BEM), using fire size and fire radiative energy (FRE) to compute the daily emission fluxes of trace gases.

- To evaluate the performance of BRAMS (using PRMv0 and PRMv1) on the vertical and horizontal distributions of carbon monoxide and ozone produced by biomass burning using airborne data from the SAMBBA (2012) campaign.

2   LITERATURE REVIEW

To introduce the context of this research, a literature review containing the major topics, such as biomass burning, plume rise physics and dynamics and numerical models used, are presented in the following subsections.

2.1.   Biomass burning in South America

During the dry season of the Southern Amazonia and *Cerrado* (savanna), specifically between July and October, large amounts of aerosols and trace gases are released to the atmosphere, emitted mainly from anthropogenic biomass burning emissions. Fire emissions include several trace gases (such as CO, CO_2, CH_x, NO_x, water vapor, volatile organic compounds, including greenhouse gases and ozone precursors, among others) and aerosols. Globally, biomass burning is responsible by producing 170 Tg of tropospheric ozone every year (JAFFE; WIGDER, 2012), which is 3.5% of all tropospheric ozone production (MONKS et al., 2014). According to Andreae (1991), South American fires inject 30 Tg year^{-1} of aerosols into the atmosphere. Though, since wildfires are strongly dependent on meteorological conditions, drought episodes and human behavior, they have a large interannual variability (DUNCAN, 2003). As most of the emitted particles are small, they can remain in the atmosphere for several days (KAUFMAN, 1995).

Using remote sensing techniques, Prins et al. (1998) determined that biomass burning smoke area over South America is, approximately, 4 to 5 mill. km^2 (PRINS; FELTZ; MENZEL, 1998). Emitted particles are composed, mainly, of partially oxidized organic matter mixed with black carbon, making them highly efficient scattering and absorbing the solar radiation. Reid et al. (1998) estimated a single scattering albedo of 0.82 for these particles. A persistent smoke layer over a tropical region can alter the Earth's energy budget and the hydrological cycle in regional or global scales. As stated by Andreae (2001), global direct radiative forcing of the black carbon is about 0.55 W m^{-2}, which is a third of the CO_2 radiative forcing. In terms of direct radiative forcing, this could

mean that black carbon is one of the most important elements in the global warming, behind only of CO_2.

Biomass burning emits hot gases and particulate material that are transported vertically upward, due to positive buoyancy. The interaction between the plume and the environment produces eddies that entrain cold air from the environment to the plume, diluting it and decreasing its buoyancy. Diurnal turbulent transport (mixing) in the planetary boundary layer (PBL) produces a well-mixed region, while horizontal advection transport the plume towards the predominant wind. Convective processes (dry and wet) and the topographic forcing, transport the emissions to the mid and high troposphere. Into the free troposphere, pollutants (emissions) are advected away from the source regions, due to stronger winds and the dominant atmospheric circulation patterns. Removal processes are more efficient within the PBL and, in contrast, when pollutants are transported to the free troposphere, their residence time increases. Several authors (ANDREAE et al., 2001, 2012; BELA et al., 2015; CHATFIELD et al., 1996; CHATFIELD; CRUTZEN, 1984; CHATFIELD; DELANY, 1990; CHATFIELD; GUO; SACHSE, 2002; FREITAS; DIAS; DIAS, 2000a, 2000b; GALANTER; LEVY, 2000; HART; SPINFAIIAE, 1999; KARL; GUENTHER; YOKELSON, 2007; LONGO; FREITAS; ANDREAE, 2009; PEREIRA et al., 2009; PICKERING; DICKERSON, 1988; THOMPSON; PICKERING, 1994) have worked with the transport of South American and African biomass burning emissions, mostly focused on deep and wet convection transport. They have shown the importance of this mechanism on the vertical distribution of the pollutants from the PBL to the high troposphere with possible implications to the regional and global climate change.

The presence of particles in the atmosphere can also alter the solar radiative balance by changing the clouds microphysics. These particles act as cloud condensation nuclei, causing changes in clouds albedo and precipitation rates (COTTON; PIELKE, 2007; ROSENFELD, 1999). This suggests that biomass burning effects can be extrapolated from the local scale to be a determinant element in the global energy distribution pattern from the tropics to mid and high latitudes, through convective transport processes.

In order to better understand the Amazon fires, is necessary to have a qualitative and quantitative description of the main characteristics of the region, as the climate, vegetation type, fire phases, etc., that are exposed next.

2.1.1. Biomass burning phases

The ignition, evolution, fire behavior and its emissions depend on several factors that are controlled by the environment. Local climate is very important on the determination of the quantity and characteristics of the biomass. For a given biomass type, the local climate, including temperature, precipitation, soil moisture, wind, etc., control the conditions to initiate the combustion process and its maintenance.

Biomass burning can be divided in four stages or phases: ignition, flaming phase, smoldering phase and extinction (LOBERT; WARNATZ, 1993). Flaming phase is a pyrolytic process, with temperatures up to 1800 K. On this stage, emitted particles are broken and decomposed from compounds with great molecular weight to minor molecular compounds, and also producing soot and tar. Nitrogen oxides, hydrocarbons and the most part of the aerosols are emitted in this phase. Carbon monoxide and other compounds with incomplete oxidation, like some aerosols, are emitted on the smoldering phase upon temperatures below 1000 K (WARD; SUSOTT; KAUFFMAN, 1992). The biomass burning moisture content determines which of the stages (flaming or smoldering) is the predominant and, besides, defines the emission ratio between CO and CO_2.

2.1.2. Amazonia and Cerrado Climate and biomass

There are differences in the amount and type of vegetation that are observed in the regions where burning happen, depending on the local climate, specifically, on the precipitation regime. In the Amazonia, there is a dense vegetation canopy, due to the fact that precipitation are more abundant and constant throughout the year, without a strong dry season, with total mean amounts between 1500 and 3500 mm per year. Meanwhile, in the *Cerrado* biome, precipitation occurs during summer of Southern Hemisphere with a dry season

in the winter. Typical annual amounts of rainfall in the *Cerrado* range from 800 to 1500 mm. Consequently, the amounts of vegetation in the *Cerrado* biome is much lower and sparser than is observed in the Amazonia. Ward et al. (1992) estimated the amount of vegetation over different areas in the *Cerrado* and Amazon biomes, stating that there is from 0.71 kg m^{-2} (*Cerrado*) up to 29.24 kg m^{-2} (Amazonia).

2.1.3. Combustion and Emission factors

The ratio between the amount of burned biomass and the total amount of biomass is called combustion factor. Depending on the type of vegetation and the fire phase, these combustion factors vary from 52 to 100% with associated standard errors from 0 to 8.2% for the *Cerrado* and 2.9 to 3.6% for the Amazon forest. In general, the higher the amount of biomass, the lower combustion factors are observed (WARD; SUSOTT; KAUFFMAN, 1992).

Another concept is the emission factor, which is the total amount of compounds emitted in terms of unit of mass of biomass burned. Estimations made by Andreae and Merlet (2001), indicate that fires in the *Cerrado* emit, in average, 1613 g[CO_2]/kg[biomass burned] and 65 g[CO]/kg[biomass burned], though for the Amazon forest, the average emission factors are 1580 and 104 g/kg for the CO_2 and CO, respectively. In addition, they observed that in the *Cerrado*, biomass is consumed mainly during the flaming phase. However, in the Amazonia, the fraction of biomass consumed during the flaming and smoldering phase was almost the same.

The estimation of the emission factors for different compounds is currently a big challenge. There are several emission inventories for biomass burning, but these are based on observed data in short-term scientific campaigns. To include these data in numerical modelling of the atmosphere, the current trend is to estimate these factors using the fire radiative power (FRP) emitted by the combustion process and measured via remote sensing (PAUGAM et al., 2015a, 2015b; PEREIRA et al., 2009). This topic is exposed in Section 2.1.6.

One of the biomass burning emission models widely used to estimate emission fluxes in tropical regions is the 3BEM (Brazilian Biomass Burning Model; LONGO et al., 2010), which uses remote sensing data to determine the fire sizes.3BEM provides of daily emission fluxes for several chemical species. This topic is described in more detail in section 2.3.2.

2.1.4. Physics and dynamics of the fire plumes

Physical processes involved in the interaction of fire plumes with the environment (Fig 2.1) are (i) buoyancy generated by the convective heat flux (CHF), caused by the fire itself and it is related to the net heat released and to the fire radiative power (FRP; FREEBORN; WOOSTER; HAO, 2008; WOOSTER et al., 2005); (ii) size of the combustion zone, which controls the surface area of the plume that interacts with the atmosphere (FREITAS et al., 2006); (iii) atmosphere stratification (KAHN et al., 2008), (iv) the quantity of turbulent mixing happening in the edge of the plume, which affects the en/detrainment of the environment and the plume (this decreases the initial upward current) (KAHN et al., 2007); (v) wind shear affects the horizontal mixing and, consequently, the en/detrainment of the environment and the plume; and (vi) the latent heat released because of water vapor condensation entrained into the plume (FREITAS et al., 2006).

2.1.5. Biomass burning monitoring

Remote sensing is the most feasible technique for monitoring biomass burning in South America, due to the large spatial distribution of the fires. Pereira (1988) and Setzer and Pereira (1991), developed a detection of hot points or fire spots for the *Cerrado* and Amazon biomes through the Advanced Very High Resolution Radiometer (AVHRR). Prins and Menzel (1992) used the Visible Infrared Spin Scan Radiometer Atmospheric Sounder (VAS) onboard of the Geostationary Operational Environmental Satellite (GOES) for monitoring biomass burning in the *Cerrado* and deforested areas. Their technique is based
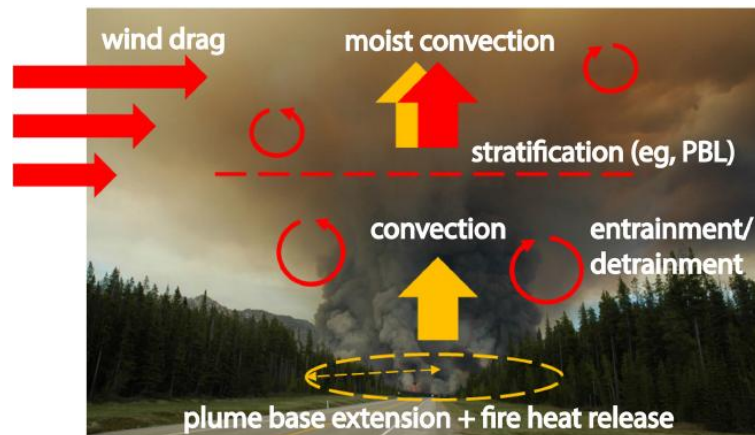
Figure 2.1 Schematic view of the physical processes involved in fire plume dynamics. Red and yellow colors stand for atmospheric or fire induced mechanisms, respectively. (adapted from Paugam et al., 2015a).

on the difference of radiative temperatures related to two infrared channels (MATSON; DOZIER, 1981). However, the low spatial resolution of the VAS instrument is a limiting factor to the monitoring of biomass burning, but in the other hand, its good temporal resolution it is a big advantage that allows to observe the diurnal cycle of active fire spots.

In 1994, the launch of GOES-8 satellite (positioned at longitude 75º W) and the implementation of the Wildfire Automated Biomass Burning Algorithm, version 1.1 (WF-ABBA), contributed to significantly improve the monitoring of the active hotspots in the 1995 fire season of South America (PRINS; FELTZ; MENZEL, 1998). GOES-8 spatial resolution at nadir is 1 km in the visible channel and 4 km in the infrared channels (3.9 and 10.7 microns). WF-ABBA was developed at the Cooperative Institute for Meteorological Studies (CIMSS, University of Wisconsin-Madison) to detect and estimate automatically the size and temperature of the fires in South America. Prins et al. (1996) made a study of the diurnal variability of the fire pixels using the WF-ABBA for the 1995 South American fire season. They observed that the higher quantity of fire pixels occurs around 17:45 UTC, and varies between 1500 and 3500 fire pixels. At this time, detected fire pixels were three or four times above the observed at 14:45 and 20:45 UTC and, approximately, twenty times higher than the fire pixels observed at 11:45 UTC. WF-ABBA allows to monitor biomass burning in several ecosystems and was simplified to a fast processing every 30 minutes to

be used in data assimilation of models. Currently, WF-ABBA is in its version 6.5.

In addition, polar orbiting satellites are used to monitor biomass burning. One of the most popular sensors used is the Moderate Resolution Imaging Spectroradiometer (MODIS), which is on board of the Terra and Aqua satellites. It has a spatial resolution of about 1 km at nadir. This is a great advantage in comparison to GOES satellites, allowing to locate the hotspots more accurately, introducing less errors in the assimilation data used by atmospheric models. However, polar orbiting satellites have a low temporal resolution in the intertropical zone, with just two daily observations: one from the Aqua satellite and other from the Terra satellite.

2.1.6. Fire Radiative Power

Currently, fire radiative power (FRP) is one of the most used parameters to estimate biomass burning emissions (PAUGAM et al., 2015a). FRP can be defined as the part of the chemical energy emitted as radiation in the biomass burning process and it can be estimated via an airborne infrared radiometer (RIGGAN et al., 2004) and, also, through infrared bands in fire data from environmental satellites such as GOES, Terra and Aqua (PEREIRA et al., 2009).

MODIS based estimates of FRP characterize the relationship between the bright temperature of the fire and the medium infrared (4 and 11 microns) pixels (KAUFMAN; TANRÉ, 1998; KAUFMAN; KLEIDMAN, 1998; KAUFMAN, 1995). Using a contextual algorithm, MODIS obtains 1 km of spatial resolution for the fire pixel (GIGLIO et al., 2003). In the same way, GOES WF-ABBA product uses two infrared channels and has 4 km of spatial resolution at nadir. WF-ABBA does not estimate FRP directly, but there are methods to obtain this physic parameter (see section 3.3).

Pereira et al. (2009) estimated trace gases and aerosols emitted by biomass burning in South America through FRP retrieved by MODIS and GOES satellites. They included that inventory in the CATT-BRAMS modeling system

and concluded that FRP estimations made by GOES algorithm overestimate the MODIS FRP estimations by a factor of three.

FRP estimations represent a significant improvement to quantify biomass burning emissions, however there are some errors and limitations to obtain it via remote sensing. GOES and MODIS fire products require complex validations that were not yet completely performed. Some uncertainties are intrinsic to the remote sensing and some factors, such as channel saturation (due to high fire temperatures), non-detected fires, cloudy skies, smoke plume effects on the estimation of FRP, regional features of the biomass burning, fire size, etc., are common.

2.2. Transport models

Nowadays, on the environmental forecast context, the main challenge of the meteorology is to simulate accurately the complex atmospheric system via numerical models that are being constantly developed and adjusted, including and testing new parameterizations, numerical schemes, etc. and updating them in terms of spatial and temporal resolutions in according to the computational development.

Several atmospheric transport models, both regional and global scales, have been used to describe and to study aerosols and trace gases emitted by biomass burning. Grell et al. (2000) described a complex multiscale chemical model coupled to the non-hydrostatic MM5 model (MM5-Chem). Chatfield et al. (1996) used the Global-Regional Atmospheric Chemistry Event Simulator (GRACES) to introduce a conceptual model of how emissions and wildfire chemistry produce the African and Oceanic plumes. Chatfield et al. (2002), showed a connection between tropical emissions and a subtropical carbon monoxide plume in remote areas over the Southern Pacific Ocean, using the GRACES and MM5 models. Chin et al. (2000), simulated the sulfur atmospheric global cycle using the Georgia Tech/Goddard Global Ozone Chemistry Aerosol Radiation and Transport (GOCART) model. Another chemistry-transport model widely used is the Model of Ozone And Related Tracers (MOZART). MOZART is appropriated to simulate the distribution of three chemical species in the

atmosphere (BRASSEUR; HAUGLUSTAINE, 1998; HOROWITZ et al., 2003). These models are often called off-line models, i.e., the transport model is initialized using the atmospheric model output, previously ran with atmospheric data assimilation. In contrast, on-line chemistry transport models have substantial advantages, because they use the same spatial and temporal resolution of the host atmospheric model, avoiding errors related to numerical interpolation. Specifically, they are suitable to feedbacks studies between the traces and the atmosphere, e.g., aerosol effects in the atmosphere radiative transfer.

Freitas et al. (2005), used a tracer transport model coupled to the Regional Atmospheric Modeling Sytem (RAMS; WALKO et al., 2000). In their work, the tracer transport simulation is made simultaneously (on-line) with the atmospheric development, resulting in a monitoring system in real time designed to forecast and study the aerosol and trace gases transport emitted by biomass burning in South American and African continents. Another example of on-line atmospheric-transport models is the Weather Research and Forecast model with Chemistry (WRF-Chem) developed by Grell et al. (2005). Grell et al. (2011) included the biomass burning emissions into the WRF-Chem, using the Brazilian Biomass Burning Emissions Model (3BEM; LONGO et al., 2010) and implementing the Plume Rise Model (PRM; FREITAS et al., 2006) to study the 2004 Alaskan wildfires. Archer-Nicholls et al. (2014) assessed the WRF-Chem for the South American fires, comparing the model results with observational data from the SAMBBA (2012) campaign (MORGAN et al., 2013). They concluded that WRF-Chem overestimate the aerosol injection heights and suggest that the cause could be the injection height computed by the Plume Rise Model (PRM). Marenco et al., (2016), used the MetOffice Unified Model (MetUM) and the Monitoring Atmospheric Composition and Climate of the European Centre for Medium-Range Weather Forecasts (ECMWF-MACC) models to evaluate aerosol distributions during the SAMBBA campaign. They concluded that both models reproduce well the magnitude and dispersion of the aerosols, as well as the plume injection heights. However, the exact position of fires was not always well reproduced. Paugam et al. (2015b) proposed a new

biomass burning plume injection height parameterization. This topic is described in the section 2.4.

2.3. BRAMS Modelling System

The Brazilian developments on the Regional Atmospheric Modeling System (BRAMS, formerly knew as the Coupled Chemistry Aerosol-Tracer Transport model to the BRAMS (CCATT-BRAMS); FREITAS et al., 2009b, 2016; LONGO et al., 2010, 2013b) is a fully coupled regional model that includes the transport and chemical module. It was designed to solve the transport of gaseous compounds and aerosol particles simultaneously with the development of the atmospheric state (using the same time step and the same physical and dynamical parameterizations). Also, it is suitable to local and regional studies of atmospheric chemistry from the Earth's surface and the lower stratosphere. BRAMS includes aqueous and gaseous chemistry, photochemical processes and dry deposition or wet removal.

CATT is an Eulerian transport model and BRAMS is an atmospheric circulation model based onto the RAMS (WALKO et al., 2000) with specific developments and parameterizations for tropical and subtropical regions (FREITAS et al., 2009).

2.3.1. Development of BRAMS

BRAMS, as described by Freitas et al. (2009b), is based on the sixth version of RAMS. RAMS is a non-hydrostatic and compressible numerical model. It completely solves the equations of Tripoli and Cotton (1982) and have a set of physical parameterizations on the state-of-art, suitable to simulate processes as surface-atmosphere exchanges, turbulence, convection, radiation and cloud microphysics.

Among BRAMS features, there are a deep and shallow cumulus set version, based on the mass flux approximation of Grell and Devenyi (2002); an off-line soil moisture estimation, based on the RAMS soil parameterization and precipitation amounts retrieved by remote sensing, which serve as initial conditions (GEAVERD; FREITAS, 2006). The convective parameterization uses

14

the turbulent kinetic energy given by the RAMS PBL parameterization, to compute the maximum distance that air parcels can ascend from their original level and, based on this, to determine whether the grid column will or will not develop the convection. In addition, soil use adaptations were made, using data from the PROVEG project (SESTINI; REIMER; VALERIANO, 2003) for South America, while for Brazil, it uses data from the RADAMBRASIL project (ROSSATO; ALVALÁ; TOMASELLA, 2002). The Normalized Difference Vegetation Index (NDVI) dataset is based on the 2001-2002 MODIS observations, processed by the Terrestrial Biophysics and Remote Sensing Lab (TBRS) converted to the BRAMS data structure. Furthermore, biophysical parameters (vegetation leaves area index, albedo, roughness, biomass capacity, soil roughness, soil parameterizations, etc.) of the RAMS model were adapted for tropical and subtropical biomes, using observations or estimations from the last field campaigns (most from the Large-scale Biosphere-Atmosphere experiment in Amazonia, LBA). BRAMS features are described in more detail in Freitas et al. (2009b, 2016).

2.3.2. CCATT-BRAMS

The Coupled Aerosol-Tracer Transport (CATT) model is a numerical system designed to simulate and study the transport and associated processes of biomass burning emissions. It is an Eulerian transport model that is fully coupled to BRAMS (FREITAS et al., 2009, 2016). Tracer transport simulation is made simultaneously (on-line) with the atmospheric state evolution, using the same time step and the same physical and dynamical parameterizations.

The general mass conservation equation (in its tendency form) used into the CATT-BRAMS is:

$$\frac{\partial s}{\partial t} = \left.\frac{\partial s}{\partial t}\right|_{adv} + \left.\frac{\partial s}{\partial t}\right|_{\substack{PBL \\ conv}} + \left.\frac{\partial s}{\partial t}\right|_{\substack{deep \\ conv}} + \left.\frac{\partial s}{\partial t}\right|_{\substack{shallow \\ conv}} + \left.\frac{\partial s}{\partial t}\right|_{chem} + W_{PM_{2.5}} \qquad (\,2.1\,)$$
$$+ R + Q_{pr}\,,$$

where s is the grid box mean tracer mixing ratio. The right terms of the equation (2.1) are the 3-D resolved transport term (advection by the mean wind), the sub-

grid scale diffusion in the PBL, the sub-grid transport by deep convection, the sub-grid transport by shallow convection, sub-grid carbon monoxide transport (treated as passive tracer), the wet removal of $PM_{2.5}$, the dry deposition applied to gases and aerosol particles and, the last term, is the source term that includes the plume rise mechanism associated to biomass burning, respectively (FREITAS et al., 2009).

CATT considers smoke aerosols as generic particles with a diameter less than 2.5 μm and average mass density of 1.35 g cm^{-3}, considering no variation of its composition and size in time. Aerosol spectral optical properties are defined following the AERONET Amazonian climatology (PROCOPIO; REMER; ARTAXO, 2003). Wet removal of aerosol particles is associated only with deep convection and coupled to the cumulus scheme of Berge (1993). Dry deposition is simulated using the resistance approach of Wesely (1989).

CATT is also coupled to the Brazilian Biomass Burning Emission Model (3BEM; Longo et al., 2010), which provides total daily data of trace gases and aerosol particles emitted by biomass burning. 3BEM emission data is also used by the PRMv0, which is embedded into the CATT in order to determine the Q_{pr} term in the equation (2.1). 3BEM is based in the approach of Freitas et al. (2005) and, basically, for each fire pixel detected, the mass of the emitted tracer is calculated through an equation that considers estimated values of biomass available for combustion on the ground, combustion and emission factors and the fire area. A combination of three fire data sources is used: (i) the GOES WF-ABBA algorithm (PRINS; FELTZ; MENZEL, 1998), (ii) the INPE's fire product, which is based on the AVHRR aboard the NOAA polar orbiting satellites series (SETZER; PEREIRA, 1991) and (iii) the MODIS fire product (GIGLIO et al., 2003). These three data sources are filtered to avoid double counting of the same fire, by eliminating additional fires within a circle of 1 km radius. 3BEM emission units are kg m^{-2} day^{-1}, giving a diurnal cycle of them through a Gaussian function centered at 18:00 UTC (FREITAS et al., 2011), which is based on the typical wildfire diurnal cycle observed in South America

(PRINS; FELTZ; MENZEL, 1998). A detailed description of the 3BEM with all its features is exposed by Longo et al. (2010) and Freitas et al. (2011).

The Chemistry CATT-BRAMS (CCATT-BRAMS; LONGO et al. (2013b) is a module of chemistry of gaseous state fully coupled to the CATT-BRAMS. Biomass burning chemical emissions are retrieved using three data preprocessor tools (PREP-CHEM-SRC; FREITAS et al., 2011), chemical mechanisms and boundary and initial conditions. CCATT-BRAMS uses a modified version of the Community Aerosol and Radiation Model for Atmosphere (CARMA; TOON et al., 1988). More details of the CCATT-BRAMS features are described in Freitas et al. (2009b), Longo et al. (2010, 2013b), Moreira et al. (2013) and Rosário et al. (2013).

As previously mentioned, CCATT-BRAMS is called only BRAMS since 2016 (FREITAS et al., 2016). So, hereafter, BRAMS refers to the CCATT-BRAMS modeling system including all its features.

2.4. Plume Rise Model

The Plume Rise Model (PRM) was developed by Freitas et al. (2006, 2009a) based on the model proposed by Latham (1994). PRM solves explicitly the biomass burning plume rise considering the environmental wind drag, using a simple 1-D model. Governing equations are based on the vertical momentum equation (2.2) (SIMPSON; WIGGERT, 1969), the first law of thermodynamics (2.3), the continuity equations for water phases (4)-(6), the gain of horizontal velocity of the plume due to drag by the ambient air flow (7) and the increase of plume radius size due to the entrainment (8), in this case amplified by the organized inflow of ambient air. More details of the formulations and parameterizations used in the equations can be found in Freitas et al. (2006, 2009a).

$$\frac{\partial w}{\partial t} + w\frac{\partial w}{\partial z} = \frac{1}{1+\gamma}gB - \ \lambda_{entr} + \delta_{entr}\ w \qquad\qquad (\,2.2\,)$$

$$\frac{\partial T}{\partial t} + w\frac{\partial T}{\partial z} = -w\frac{g}{c_p} - \ \lambda_{entr} + \delta_{entr}\ (T - T_e) + \ \frac{\partial T}{\partial t}_{\ micro} \qquad (\,2.3\,)$$

$$\frac{\partial r_v}{\partial t} + w\frac{\partial r_v}{\partial z} = - \lambda_{entr} + \delta_{entr} \ (r_v - r_{v_e}) + \ \frac{\partial r_v}{\partial t}\bigg|_{micro} \qquad (2.4)$$

$$\frac{\partial r_c}{\partial t} + w\frac{\partial r_c}{\partial z} = - \lambda_{entr} + \delta_{entr} \ r_c + \ \frac{\partial r_c}{\partial t}\bigg|_{micro} \qquad (2.5)$$

$$\frac{\partial r_{ice,rain}}{\partial t} + w\frac{\partial r_{ice,rain}}{\partial z}$$

$$= - \lambda_{entr} + \delta_{entr} \ r_{ice,rain} + \ \frac{\partial r_{ice,rain}}{\partial t}\bigg|_{micro} + sedim_{ice,rain} \qquad (2.6)$$

$$\frac{\partial u}{\partial t} + w\frac{\partial u}{\partial z} = - \lambda_{entr} + \delta_{entr} \ (u - u_e) \qquad (2.7)$$

$$\frac{\partial R}{\partial t} + w\frac{\partial R}{\partial z} = \ ^3{}_5\lambda_{entr} + ^1{}_2\delta_{entr} \qquad (2.8)$$

Here, w, T, r_v, r_c, r_{rain} and r_{ice} are the vertical wind, air temperature, water vapor, cloud, rain and ice mixing ratios, respectively, and are associated with in-cloud air parcels. Horizontal wind u represents the center of mass of the plume at the level z. In equation (2.2) γ is 0.5, and was introduced to compensate for the neglect of non-hydrostatic pressure perturbations (SIMPSON; WIGGERT, 1969), g is the acceleration due to the gravity and B is the buoyancy term related to the difference of temperature between the in-cloud air parcel and its environment and includes the downward drag of condensate water. In this equation system, the *micro* index refers to microphysical processes and all the other variables refer to the center of mass of the plume. The term λ_{entr} denotes the lateral entrainment, given by:

$$\lambda_{entr} = 2 \propto R^{-1} \ w \ , \qquad (2.9)$$

where R is the plume radius and α is 0.05. During windy environment conditions, the relative horizontal motion between the plume and the ambient air enhances the lateral entrainment through a "collisional" process promoting and additional exchange of momentum, energy, water, trace gases and aerosols between both air masses. In this model, an instantaneous mixing between plume properties and the ambient inside it is assumed. To reproduce

quantitatively this process, Freitas et al. (2010), introduced a dynamic entrainment term:

$$\delta_{entr} = 2(u_e - u)(\pi R)^{-1} \qquad\qquad (\,2.10\,)$$

which is proportional to the difference between magnitudes of the horizontal velocity of the environment and the plume, because there is no exist dynamical entrainment when both parcels move at the same velocity. In addition, this term is inversely proportional to the plume radius, i.e., the bigger plume radius, the less plume sensitivity to this entrainment process. The derivation of this formulation is described in Freitas et al. (2010).

Microphysical parameterizations are based on Kessler (1969) for the cloud growth and includes ice formation according to Ogura and Takahashi (1971). PRM assumes a condensation nuclei concentration into the pyro-Cb of 10^5 m^{-3}, following Andreae et al. (2004). Those parameterizations provide of the microphysical terms in the equations (2.3)-(2.6).

PRM was designed to be embedded into each grid column of a 3-D host model. In this technique, the host model feeds the PRM with the environmental conditions. Since this technique has been applied to low resolutions 3-D models (grid scales greater than 20 km), it has been assumed that the fires have no significant effect on the dynamics and the thermodynamics at this scales. Of course, the absorption of radiative energy by smoke can provide feedbacks on the larger scale, but there is no way to resolve sub-grid no homogeneities introduced by fresh plumes in this model. PRM computes a plume injection layer based on the minimum and maximum convective heat flux established for three different biomes: tropical forest, savanna and pasture.

Sensitivity studies made using PRM (FREITAS et al., 2006, 2010) showed the importance of including this plume rise mechanism into 3-D chemistry transport models (CTMs). Without including it, CTMs overestimate the quantity of trace gases and aerosols in the planetary boundary layer (PBL), leaving the free troposphere completely clean, in contrast as identified in remote sensing observations. Because of this, PRM already is embedded into several CTMs, as

the BRAMS (FREITAS et al., 2009, 2016; LONGO et al., 2010, 2013) and WRF-CHEM (GRELL et al., 2011; PFISTER; AVISE; WIEDINMYER, 2011; SESSIONS et al., 2011).

2.4.1. PRMv1

Keeping the core equations, structure and definitions of the PRMv0, Val Martin et al. (2012) derived an scheme to estimate the fire convective energy directly through the fire radiative power (FRP) measured by MODIS satellites (JUSTICE; VERMOTE; TOWNSHEND, 1998). They compute the convective energy by multiplying the FRP data by a beta factor (β = 5), instead of estimate it from the vegetation type. In this version, the plume injection height is defined as a single height and not as a combination of two limits (lower and upper) as in the PRMv0.

2.4.2. PRMv2

Paugam et al. (2015b) developed the version 2 of the PRM (PRMv2), adding a conservation of mass equation, a new entrainment scheme and modifying the β factor used to convert from FRP to convective energy. They used the Collection 5 of MODIS active fire product for fires detected in North America in 2003 and comparing them with plume tops from the Multi-angle Imaging SpectroRadiometer (MISR) sensor to optimize their parameters

Regarding to the re-acceleration effect that the plume may have, due to the latent heat generated by the water vapor entrainment as the plume rise through a colder air, Paugam et al. (2015b), introduce a new prognostic variable: $\zeta = \rho R^2$, where $R(z)$ is the plume radius and $\rho(z)$ is the air density. They also include an equation for the passive scalar transport, in terms of mixing ratio of the trace (ϕ). Thus, PRMv2 is based on five prognostic variables: ϕ, ζ, w, T and u (equations (2.2), (2.3), (2.7), (2.11) and (2.12)):

$$\frac{\partial \zeta}{\partial t} + w \frac{\partial \zeta}{\partial z} = -\zeta \frac{\partial w}{\partial z} + w\zeta \ \lambda_{entr} + \delta_{entr} \ . \qquad (2.11)$$

$$\frac{\partial \phi}{\partial t} + w \frac{\partial \phi}{\partial z} = -w \ \lambda_{entr} + \delta_{entr} \ \ \phi - \phi_e \ . \qquad (2.12)$$

In the equation (12), the plume density is assumed as the same as the ambient density computed using the ideal gas law.

To close this equation system, the boundary conditions are defined on the slip ($z = 0$, with $u = 0$), and are open at the top, and the ambient atmospheric profiles of pressure, temperature, humidity and horizontal wind velocity are taken from the 3-D host model.

The end point of the time integration is controlled the variation of the dry air mass in the plume ($M_p = \int_{z=0}^{z_{max}} \zeta \, dz$). When the mean of the relative variation of M_p over the last 10 time steps is lower than 2×10^{-5}, the plume is considered to be in a steady state. The final plume injection height is defined as the altitude layer where the ratio of detrainment mass in the level and the maximum detrained mass in the integration is greater than 0.5 (13) and where there is the highest net detrained mass.

$$M_{detr} \; M_{detr}^{max} > 0.5 \qquad\qquad (\,2.13\,)$$

PRMv2 maintains the same vertical resolution of its previous versions (100 m), the time step defined according the Courant-Friedrich-Lewy criterion and the same microphysics described in Freitas et al. (2006b). More details about derivation of the equations used in the PRMv2 can be found in Paugam et al. (2015b).

3   DATA AND METHODS

The aim of this study is to evaluate the distribution of biomass burning emissions over South America with trace gases and aerosol data from the South American Biomass Burning Analysis (SAMBBA, 2012) field campaign. This campaign took place in the Amazonia and *Cerrado* biomes in Brazil from 14 September to 3 October 2012, which is the same data used for the studies and analysis. In the following subsections, detailed information about the data sources and methodologies applied are described.

3.1.   PRM offline evaluation

As a previous work of this study, a partial and simple reproduction of Paugam et al. (2015) results were made, to verify and understand the improvements on PRMv2. The same data used by them were used, this is fire radiative power (FRP) and burnt area from the collection 5 MODIS active fire product (GIGLIO et al., 2003) for fires detected in North America in 2003. Ambient atmospheric profiles of pressure, temperature, humidity and wind for every fire cluster from ECMWF analysis runs were used to serve as boundary conditions for PRM. This atmospheric data is re-sampled to a 1.0° resolution horizontal grid and contains 60 levels with similar vertical resolution near the ground (~10m) gradually stretched up to the top of the domain located at 65 km. Therefore, off-line runs using the three different versions of PRM were made for all detected fires and the results were compared between them. In the PRMv2, the optimized values suggested by Paugam et al. (2015) were used to convert from FRP to convective heat flux (CHF; CHF = 0.88 FRP).

3.1.1. PRM configuration

PRM lower boundary condition is based on a virtual source of buoyancy placed below the model surface (LATHAM, 1994; TURNER, 1979). Buoyancy generated by this source is obtained from the convective energy flux (CHF) and the plume radius. In the original version of PRM (PRMv0), the CHF is derived for each grid column, where all fires are aggregated into three categories (forest, woody savanna and grassland) by merging the fire location with the land

use dataset. For each category, two heat fluxes (lower and upper limits) are defined according to Freitas et al. (2006a) and using a factor of 0.55 to convert the CHF into convective energy (MCCARTER; BROIDO, 1965). The plume radius is estimated through the fire size, retrieved by remote sensing. The area of the fire is defined from the simple mean of the instantaneous size of all fires that belong to the same category. In PRMv1 and PRMv2, the CHF is computed by using FRP information multiplying it by a β factor (Table 3.1). In PRMv1, β equals to 5 (VAL MARTIN et al., 2012) and in PRMv2 β = 0.88 (PAUGAM et al., 2015b).

The upper boundary condition of the three versions is defined by a Rayleigh friction layer with 60 s timescale, which relaxes wind and temperature toward the undistributed reference state values. The Arakawa-C grid is used and the model grid space resolution is 100 m with a top at 20 km height. The model time-step is dynamically calculated following the Courant-Friedrich-Lewy stability criterion, not exceeding 5 s. Microphysics is resolved with the time splitting (a third of the dynamic step). The heating rate increases linearly in time from 0 to its prescribed value at time equal to 50 min, this number being the upper limit of the time integration for PRMv0 and PRMv1. The final rise of the plume is determined by the height in which the vertical velocity of the in-cloud air parcel is less than 1 m s^{-1}. Note that for PRMv2, the final time of integration, is controlled by the detrained air mass into the plume, as described in section 2.4.2.

In this study, we suggest a similar version of PRMv1, in which the main difference is the β value to convert from FRP to CHF. In this suggested version, β equals to 0.88 (Table 3.1).

3.2. Observational data sets

In this study, BRAMS model results are compared against various remote sensing data sets. The Tropical Rainfall Measuring Missions (TRMM) is a NASA project aiming to provide satellite derived estimates of tropical precipitation across the globe. The 3B42 product produces 3-hourly merged with high

quality, infrared and microwave precipitation estimates at 0.25° × 0.25° resolution between 50° N and 50° S (HUFFMAN et al., 2001).

The Moderate Resolution Imaging Spectroradiometer (MODIS) instrument, on board the two NASA satellites Aqua and Terra, provides measurements of aerosol optical depth (AOD) across a wide spectral range at 1.0° × 1.0° (REMER et al., 2005). For this study, retrievals of AOD at 550 nm were used to verifying the model aerosol horizontal distribution. Overpasses over the Amazon in the study period were approximately 05:30 and 17:30 UTC for the Aqua satellite and 02:30 and 14:30 UTC for the Terra satellite. Model data was extracted at these times when comparing against MODIS data. Over land, the MODIS AOD retrievals have an error of ~0.05 (REMER et al., 2005).

3.3. Fire data

For initialization, all three versions of PRM need of the atmospheric boundary conditions (temperature, pressure, humidity and horizontal wind velocity) provided by BRAMS, the fire size and, for the case of PRMv1 and PRMv2, the FRP data from remote sensing. Fire size and FRP data from GOES-13 and MODIS satellites were used from its fire products (WF-ABBA and MODIS active fire product). In this study, the fire data was processed following Pereira et al. (2009) methodology.

The MODIS sensor estimates FRP (in MW) through the method first developed by Kaufman and Kleidman (1998) and Kaufman et al. (1996, 1998) and characterizes the relationship between the brightness temperature of fire and background pixels in the middle infrared (~4 µm), given by:

$$FRP_{MODIS} = 4.3 10^{-19}(T_{f4\mu m}^8 - T_{b4\mu m}^8)A_{sampl} \qquad (\,3.1\,)$$

where $T_{f4\mu m}$ and $T_{b4\mu m}$ are the MODIS brightness temperature of the fire pixel and the non-fire background in Kelvin (K), respectively. A_{sampl} stands for the real area of the pixel (km^2).

Table 3.1 Summary of Plume Rise Model versions used in this study and the main differences between them. Note that the convective heat flux is computed following the relationship CHF = FRP × β for all versions, except for the PRMv0.

Version	Features	β value
PRMv0	Main version developed by Freitas et al (2007, 2010). Uses fixed values (min. and max.) of convective heat flux according the biome.	-
PRMv1.0	Uses FRP to compute the convective heat flux (Val Martin et al., 2010). It keeps the core equations of PRMv0.	5
PRMv2	Uses FRP to compute the convective heat flux (Paugam et al., 2015b). Also has developments on the conservation of mass and en/detrainment.	0.88
PRMv1.1	Hybrid between PRMv1.0 and PRMv2 suggested in this study. It uses a β value suggested by Paugam et al. (2015b) and the same estructure of PRMv1.0	0.88

The WF-ABBA/GOES products do not include a FRP estimation, however it can be calculated by using:

$$FRP = A_f \sigma T_f^4 \qquad\qquad (3.2)$$

where A_f represents the fraction of fire in the pixel (m), σ is the Stefan-Boltzmann constant and T_f is the fire temperature. The area and the temperature of fire are derived using the method described by Dozier (1981). Although, GOES FRP overestimate MODIS FRP by three times, the new GOES FRE-based smoke aerosol emission coefficients could minimize FRP sensor measurement differences by introducing an external variable as a correction factor for satellite-derived emission estimation (PEREIRA et al., 2009).

The temporal integration of FRP gives the fire radiative energy (FRE) used to generate the emission fluxes of the chemical species estimated by the 3BEM version suggested in this study (3BEM-FRE). In the 3BEM-FRE, the biomass burned parameter for every grid box with fires is given by the mean FRE of the detected fires multiplied by 0.75. This value, called enhancement factor, was stablished by comparing generated emission fluxes with the previous version. Then, the 3BEM model uses the biomass burned to compute the combustion and emission factors for every chemical specie. Thus, using MODIS and GOES fire products, daily fire emission fluxes in each fire pixel were estimated and

inserted in the model. The original 3BEM version does not uses FRE information to compute the emission fluxes for the chemical species.

3.4. BRAMS model configuration

A modified version of the BRAMS version 5.2 was used in this study. Developments are focused in the inclusion of the three new versions of the PRM (PRMv1.0, PRMv1.1 and PRMv2). Runs were made using with the four versions of the PRM (Table 3.1), with initial and boundary atmospheric conditions from the GFS model, and, for the chemical conditions, the climatology from the MOCAGE was used. Both using spatial resolutions of 0.5° of latitude (~55 km). A *spin-up* of 15 days prior to the date of simulation (14 September 2012) was made to assure the steady state of the initial conditions, due to the chemical initial and boundary data need several days of simulation to reach the steady state. BRAMS main setup is showed in Table 3.2.

Simulations were made recycling the tracers of the previous day and restarting from the boundary conditions and last analysis of the model every 24 hours, until the last day of simulation (30 September 2012).

Daily chemical emissions from urban, biogenic and biomass burning were used in the initialization of the model. These emissions were generated by using the PREP-CHEM-SRC (FREITAS et al., 2011) by its version 1.5, collecting data from RETRO, EDGAR (HTAP), SEAC4ARS and MEGAN inventories.

3.5. SAMBBA campaign data analysis

The SAMBBA aircraft campaign was based in Porto Velho, RO, which is a region with extensive biomass burning owing to forest clearance. Twenty flights were conducted between the 14 September and 3 October 2012, encompassing an extensive geographic area and differing synoptic conditions (see ARCHER-NICHOLLS et al. (2014), for further details). Flights over the western regions encompassed two meteorological regimes as discussed in Brito et al. (2014), with Phase 1 (13-22 September 2012) representative of dry

Table 3.2 BRAMS 5.2 main configurations used in this study.

Parameter	Value
Number of points in X direction	387
Number of points in Y direction	360
Levels in Z	45
Vertical coordinate	Sigma-z
Grid spacement (X and Y)	20 km
Time step	30 s
Domain center Latitude	19.0° S
Domain center Longitude	54.4° W
Chemistry	Rosenbrock "RODAS3" 3rd order
Plume rise model update frequency	20 min
Deep cumulus parameterization	Grell & Deveny (2002) scheme
Shallow cumulus parameterization	Grell & Deveny (2002) scheme
Microphysics parameterization	Single moment Bulk scheme (WALKO et al., 1995)
Radiation parameterization	Carma (TOON et al., 1988)
Monotonic advection	Walcek 1st order
Ratio of minimum horizontal eddy viscosity coefficient	-0.6

season conditions and Phase 2 (22-30 September 2012) of the transition to the wet season. Flights selected to analysis were those who have the aim to measure smoke plumes, as represented schematically in figure 3.1.

Airborne carbon monoxide and ozone measurements were made every 1 second (1 Hz) and only the data with good quality was considered. This data was filtered by computing the average and the standard deviation every 5 min, to compare then with the model outputs. Georeferenced CO and O_3 data were used to compare against the model simulations made with every PRM version.

In addition, averaged vertical profiles (every 50 m) were compared against model results. This was made considering the entire valid dataset for every selected flight. Then, the aircraft path was set as an area in which the averaged model data was extracted. Using the same flights, a comparison between the observed values of CO and O3, versus the model results, to obtain a correlation between both scenarios.
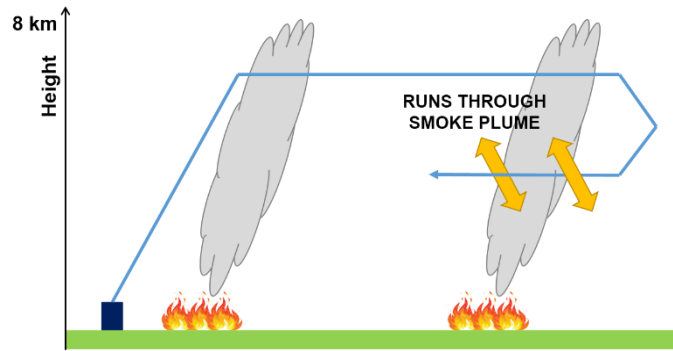
Figure 3.1 Idealized flight pattern for the SAMBBA flights with the aim to study smoke plumes. The dark blue box represents the point of takeoff and the blue arrow shows the aircraft trajectory.

Two flights with LIDAR (Light Detection and Ranging) aerosol measurements were used (flights 733 and 743), representative of the phase 1 and phase 2 of the SAMBBA campaign. The aerosol data presented here have a vertical resolution of 45m and an integration time of 1min. This integration time corresponds to a 9±2 km footprint, at typical aircraft speeds. Lidar signals within 300m of the aircraft have been discarded, due to incomplete overlap between the emitter and the receiver field-of-view, and at the far end profiles have been truncated to remove the surface spike and any data beyond it. As a general rule, a vertical profile where a cloud was detected has either been omitted completely, or has been omitted in the portion between the surface and the cloud top. However, in a small number of cases where the cloud optical depth has been considered sufficiently small, so as to not affect the derivation of aerosol properties. More details about the LIDAR aerosol data can be found in Marenco et al. (2016).

Comparison between the LIDAR aerosol data, as aerosol extinction coefficient, was compared against model results using the carbon monoxide, assuming that the CO has a distribution and dispersion very similar with aerosol particles of a typical size as the emitted by biomass burning.

4 RESULTS AND DISCUSSION

The first part of this research consist in to a partial reproductions of the results exposed by Paugam et al. (2015b). This was made with some differences in the methodology applied, specifically, the filters used to select fires to analyze. This is because the relevant results for this research does not address all the items exposed by them. The aim of this first part was to extend the knowledge on the new developments of the PRMv2 and its parameters to compare the results with the previous versions. The results are showed in the next subsection.

4.1. PRM performance over North America

In 2003, 39476 fires were detected by the Moderate-Resolution Imaging Spectroradiometer (MODIS), in the region limited between latitudes 35⁰-70⁰ N and longitudes 40⁰-170⁰ W. This is the Collection 5 of MODIS active fire product dataset (GIGLIO et al., 2003). In the same way as Paugam et al. (2015b), only 30951 runs were made, because the remaining cases had Fire Radiative Power (FRP) and/or burnt area errors. Although, they only ran for 19804 cases when using the PRMv2.

Following the methodology of Paugam et al. (2015b), only fires with a burnt area higher than 1 ha; and cases which the simulated injection height (InjH) were higher than the planetary boundary layer (PBL) height were selected for analysis. The differences in the methodology applied in this work were:

a) the distinction among different cases with stable or unstable atmosphere was not applied; and

b) two runs for each fire using the PRMv0 were made: one of them considering a convective heat flux (CHF) of 30 kW m^{-2} and the other using 80 kW m^{-2}. These values were defined by Freitas et al. (2006), as minimum and maximum values of CHF, respectively, for tropical and boreal forests.

Table 4.1 Number of plume injection heights predicted by the three versions of Plume Rise Model for the fires detected in North America in 2003 by the Moderate-Resolution Imaging Spectroradiometer (MODIS) and reported in its collection 5 of the active fire product. Heights are above ground level.

Model	Number of plumes				Max. plume height (m)
	< 4km	> 4 km	> 6 km	> 8 km	
PRMv0 (30 kW m^{-2})	8 731	57	7	8	12 800
PRMv0 (80 kW m^{-2})	7 466	235	23	18	18 600
PRMv1	7 584	119	13	11	11 000
PRMv2	7 153	649	177	71	11 100

The results are in agreement with the work of Paugam et al. (2015b), even though with the differences in the methodology to select the analyzed cases. In general, plumes had greater development in the runs made with PRMv2, reaching higher tops than the other versions (Table 4.1). That means that PRMv2 can reproduce Pyro-Cumulonimbus (Pyro-Cbs) plumes better than the previous versions. Fromm et al. (2010) observed 17 Pyro-Cbs with top plume heights between 9.5 and 13 km in this same dataset. Comparing this with our and Paugam et al. (2015b) results, only PRMv2 predictions are closer to these observations. In addition, PRMv1 could replicate, in part, those observations, showing 11 Pyro-Cbs plume type. PRMv0 runs (using a CHF of 80 kW m^{-2}) simulated 18 Pyro-Cbs, with a maximum top at 18.6 km. In contrast, the same version, but using a CHF of 30 kW m^{-2}, showed 8 Pyro-Cbs plume type. This is due the CHF value used, which is distributed in the same fire area in each run, and it is directly related to the plume top.

As discussed in Paugam et al. (2015a), the main lack of the previous versions of PRM and the plume rise parameterization by Sofiev et al. (2012), was the difficulty to reproduce higher plumes. In table 4.1, note that PRMv2 is the main version that is able to reproduce plumes higher than 4 km. This is associated to the diverse improvements on the model.

In the other hand, Archer-Nicholls et al. (2014), using the PRMv0 with the WRF-Chem model over South America, found that PRMv0 is actually overestimating the wildfire plume tops when compared to the SAMBBA campaign data observations, because most of the biomass burning plume injection heights are

about 1 to 2.5 km above the surface. If PRMv2 is developing higher top plume heights, this could be an issue to study in more detail and, maybe, would be necessary to adjust some of the optimized parameters established by Paugam et al., (2015b).

The relationship between plume tops and the burnt area of each fire is showed in figure 4.1. Results show a clear tendency, the higher burnt area, the higher top plume heights. This is observed in the three versions of the PRM tested. Figure
4.1, also highlights that the coefficient of determination (R2) is greater, but low (0.08-0.15), for the PRMv0 than for the other versions. In fact, the lower R^2 value recorded was for the PRMv2 runs (0.04). This can be explained because PRMv2 does not use only the burnt area and CHF parameters to determine the final plume injection height, but also uses another entrainment parameters and unfixed CHF values (converted through FRP retrieved via remote sensing data) for each individual fire. Thus, the burnt area is less relevant for the final injection height computed, but with the energy of the fire, more in accordance as it happens in reality.

In the same way, the higher FRP, the higher is the plume injection height modelled (Fig. 4.2). Dependence between top plume height and FRP is greater for the PRMv2 (R^2 = 0.37) than for the PRMv1 simulations. This shows that the improvements added to the PRMv2, in terms of converting FRP to CHF for each individual fire. Cases for both PRMv0 runs are not showed since they do not use FRP data for its initialization.

In summary, results replicated in this work, based on of Paugam et al. (2015b), show several similarities with their, even having light differences in the methods used to filter data and having greater number of analyzed fires. This results reveal the improvements made on the PRMv1 and PRMv2 in the estimation of plume injection heights, especially, for the big fires (> 1 ha) that reach the middle and higher troposphere (Pyro-Cbs).
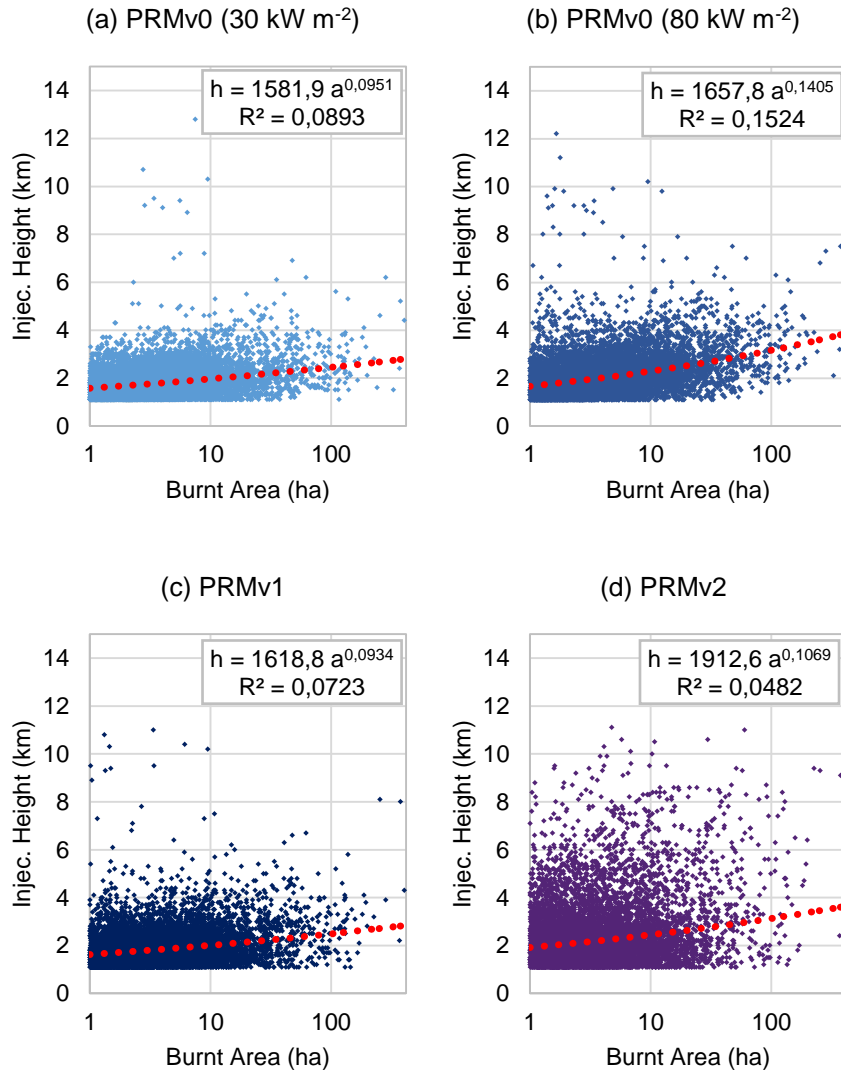
Figure 4.1 Relationship between modelled plume injection height and burnt area, for fire plumes reaching the free troposphere. The injection heights are shown estimated using the three versions of the Plume Rise Model: (a) PRMv0, with CHF = 30 kW m^{-2}; (b) PRMv0, with CHF = 80 kW m^{-2}; (c) PRMv1 and (d) PRMv2. Fires are those detected by the Collection 5 MODIS Active Fire Product for 2003 over North America (GIGLIO et al., 2003). For each plot, the best-fit relationship between plume height (h) and burnt area (a) is shown as the red dotted line. In addition, the coefficient of determination (R^2) is informed. Injection heights are reported as height above ground level (km).

Another important issue for numerical modelling is the time of computation needed by every PRM version. PRMv0 and PRMv1 had almost the same time: 0.7 hours to compute ~20000 fires of the dataset, meanwhile PRMv2 used

(a) PRMv1   (b) PRMv2

$h = 1080,8\ FRP^{0,1021}$
$R^2 = 0,2175$

$h = 802,95\ FRP^{0,1873}$
$R^2 = 0,3705$
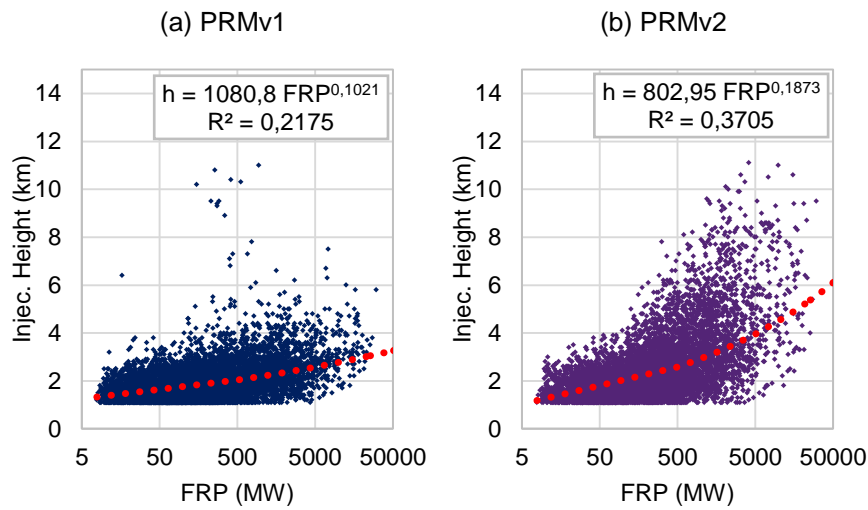
Figure 4.2   Relationship between modelled plume injection height and FRP, for fire plumes reaching the free troposphere. The injection heights are shown estimated using the versions of the Plume Rise Model that use remote sensing data for its initialization: (a) PRMv1 and (b) PRMv2. Fires are those detected by the Collection 5 MODIS Active Fire Product for 2003 over North America (GIGLIO et al., 2003). For each plot, the best-fit relationship between plume height (h) and FRP is shown as the red dotted line. In addition, the coefficient of determination (R^2) is informed. Injection heights are reported as height above ground level (km).

about 10 times more time to compute the InjH for the same fires. For weather and air quality forecasts, this is an important matter to put attention in, due to there are 15000 fires detected every day in South America during the fire season.

In the next sections, results of PRM performance over South America, using the BRAMS modelling system, are presented and discussed. Then, is made the model evaluations using the SAMBBA (2012) field campaign data.

As stated in the section 2.4.1, PRMv2 computes the plume injection height for every individual fire. Nowadays. in numerical modeling of the atmosphere, is it necessary to use a grid spacing above 1 km in the mesoscale. In this work, a 20 km resolution grid was used for South America. Since could be more than a single fire into a grid box, the computation of PRMv2 module into the BRAMS model would have been too long. Because of that, PRMv2 was not used into the BRAMS simulations and the runs were made using the original PRMv0 and

two different variations of PRMv1. These variations were based on modifying the conversion factor used to compute the fire convection heat flux (CHF): PRMv1.0 maintains the same conversion factor described by Val Martin et al. (2012), this is $\beta = 5$; PRMv1.1 uses the conversion factor recommended by Paugam et al. (2015b) for the PRMv2, this is $\beta = 0.88$.

4.2. Rainfall during the SAMBBA campaign

Climatology, the wet season in southern Amazonia and *Cerrado* starts in late September, due to the progressively coming of the summer, generating the propitious meteorological conditions to develop deep convection in the region. Both TRMM measurements and BRAMS runs shows the differences between the two phases of the SAMBBA campaign (Fig. 4.3). Phase 2 is much wetter in southern Amazônia than in the phase 1. During phase 2, TRMM estimates accumulates about 50 mm in this area, meanwhile, during phase 1, about 30 mm. In both phases, BRAMS model is overestimating the total precipitation. This is very difficult to discuss, because is well known the difficult of TRMM products on estimating the precipitation due to warm clouds. Indeed, in Amazônia, an appreciable amount of precipitation is of this kind. It is necessary to know an accurate proportion of what percentage of the precipitation in Amazônia is due to warm clouds to evaluate the model behavior. In general terms, BRAMS represents very well the structures of rain (location) observed in South America during the campaign.

4.3. Fire properties during the SAMBBA campaign

Fires have a larger extension (Fig. 4.4) and release more energy (Fig. 4.5) during the Phase 1 than in the Phase 2 of the SAMBBA campaign. This is due two main reasons: (i) the first phase is characterized by dry meteorological conditions making the propitious environment for fire develops, (ii) during the phase 2, *Cerrado* continues dry (as showed in Fig. 4.3), but the amount of biomass available to burn is much lower than in the Amazônia. Because of this, there are many fires, but they did not reach large sizes and, consequently, are not too powerful as the fires observed in the Amazônia during the phase 1.
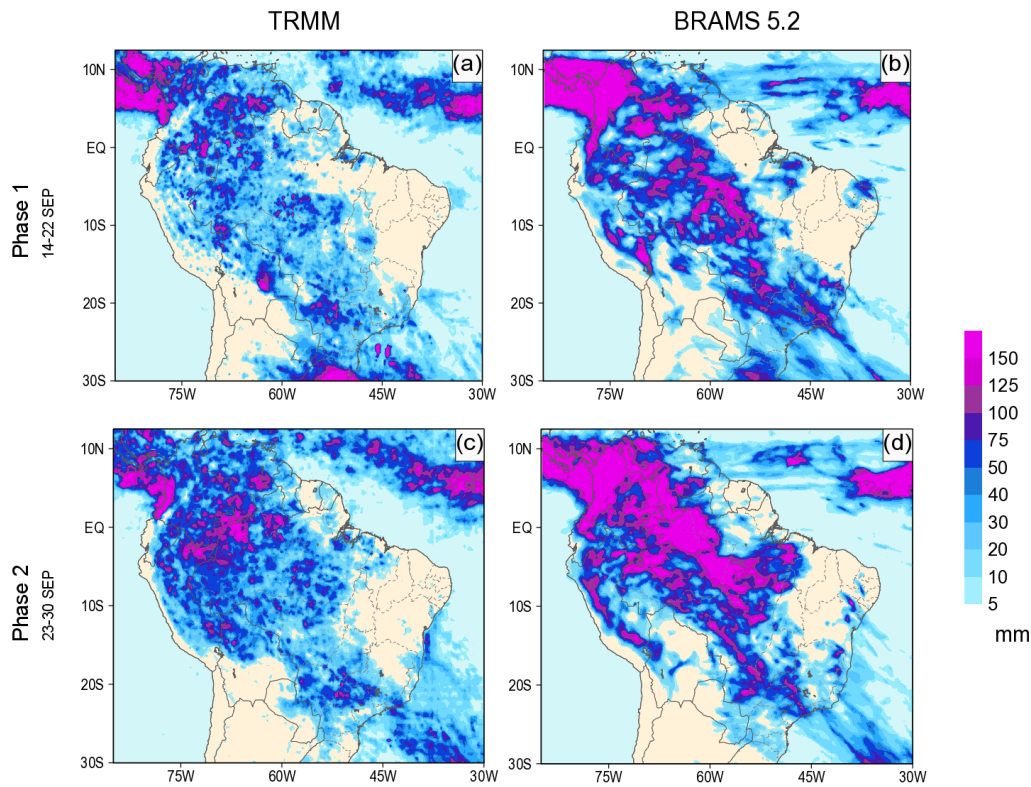
Figure 4.3 Accumulated precipitation (mm) during the Phases 1 (14-22 September; a and b) and 2 (23-30 September; c and d) of the SAMBBA (2012) campaign. Panels (a) and (c) shows the TRMM 3B42 (Huffman et al. 2001) observations and panels (b) and (d) shows the BRAMS model runs.

Mean fire sizes as big as 100 ha or more were detected in the state of Rondônia and Tocantins. These fires are directly correlated to the biome where they occur and the FRP of them. The largest fires had measurements of FRP of several thousands of MW. As we are using the FRE (derived from FRP measurements) to compute the emission fluxes in the 3BEM model, we filtered this data. A maximum of FRP was set to 4000 MW. All fires with a FRP greater than 4000 were reduced to this fixed value, to not have unrealistic biomass burning emissions.

4.4. 3BEM developments

One of the aims of this work is to implement a new scheme to produce the biomass burning emissions in the 3BEM model made by Pereira et al. (2009),
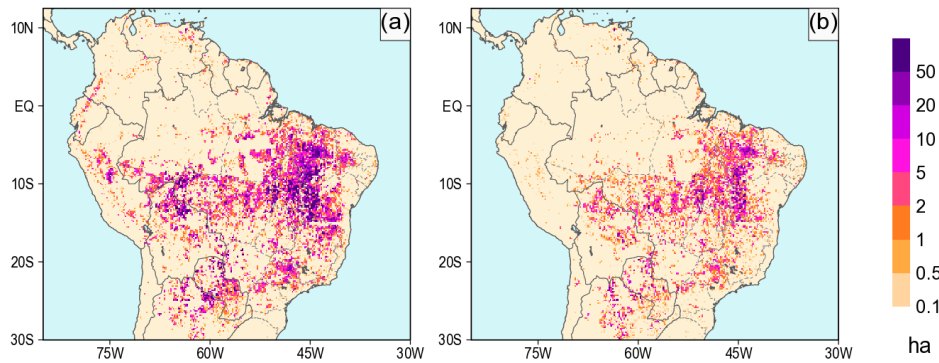
Figure 4.4 Average fire size (ha) of the fires detected during (a) Phase 1 (14-22 September 2012) and (b) Phase 2 (23-30 September 2012) of the SAMBBA campaign, retrieved from the MODIS and GOES fire products.
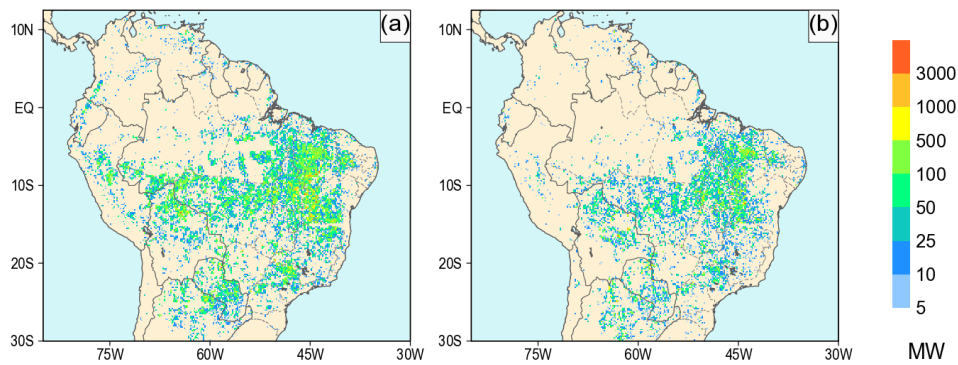
Figure 4.5 Average fire radiative power (FRP, MW) of the fires detected during (a) Phase 1 (14-22 September 2012) and (b) Phase 2 (23-30 September 2012) of the SAMBBA campaign, retrieved from the MODIS and GOES fire products.

hereafter 3BEM-FRE, which uses fire size and FRP (to derive the FRE) measurements from remote sensing to compute the daily biomass burning emission fluxes.

Results show that the 3BEM-FRE is producing larger amounts of carbon monoxide (and other chemical species not showed) than the traditional formulation (Fig. 4.6). Both are generating greatest emissions in concordance with the location of the bigger fires discussed in the previous section. Emission
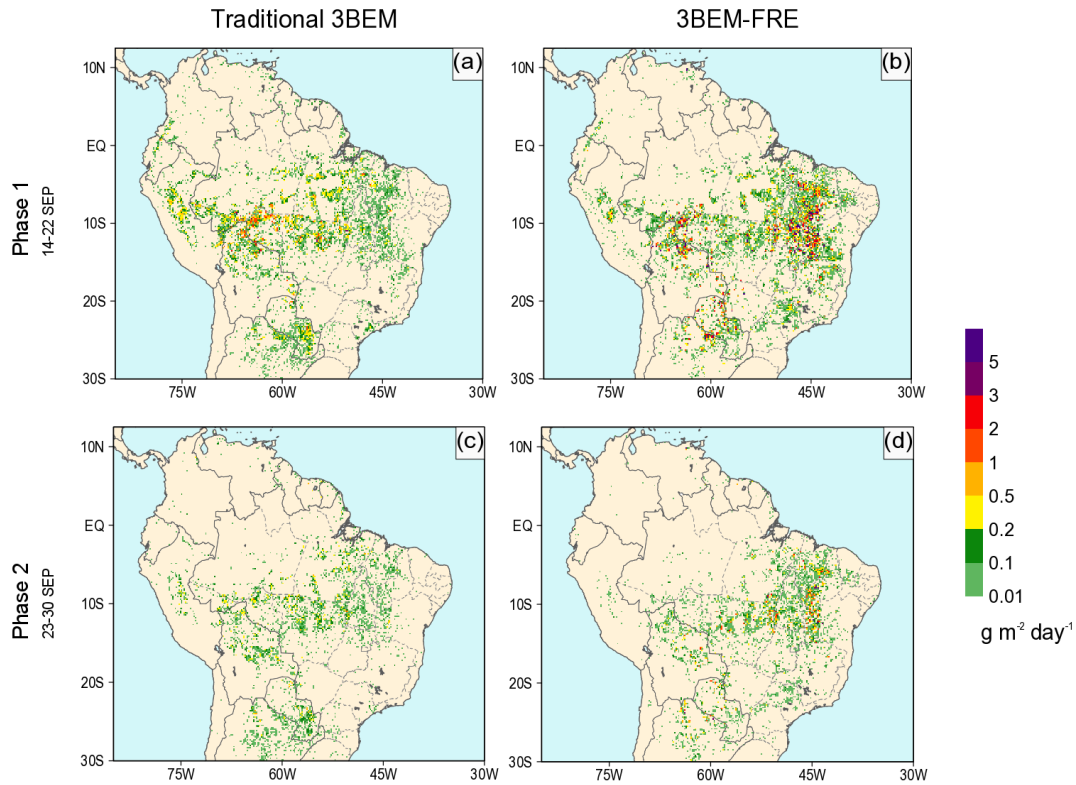
Figure 4.6 Emission fluxes of carbon monoxide (g m^{-2} day^{-1}) during the Phases 1 (14-22 September; a and b) and 2 (23-30 September; c and d) of the SAMBBA (2012) campaign. Panels (a) and (c) show the emission fluxes using the traditional formulation of the 3BEM and, panels (b) and (d) show the emissions using the new scheme suggested in this study (3BEM-FRE).

fluxes of CO are larger in the first phase of the campaign than in the second, because of the dry meteorological conditions that lead to have more fires than in the second part of the campaign (dry-to-wet transition).

4.5.   SAMBBA flights and model results

The SAMBBA flights used in this study are shown in the table 4.2 and their trajectories in figure 4.7. The six flights selected are those that their aim was to measure the biomass burning emissions passing through the plumes several times. Five of the six flights took place in the Amazon forest and areas with deforestation, except for the flight 742, which sampled fires in the *Cerrado*.
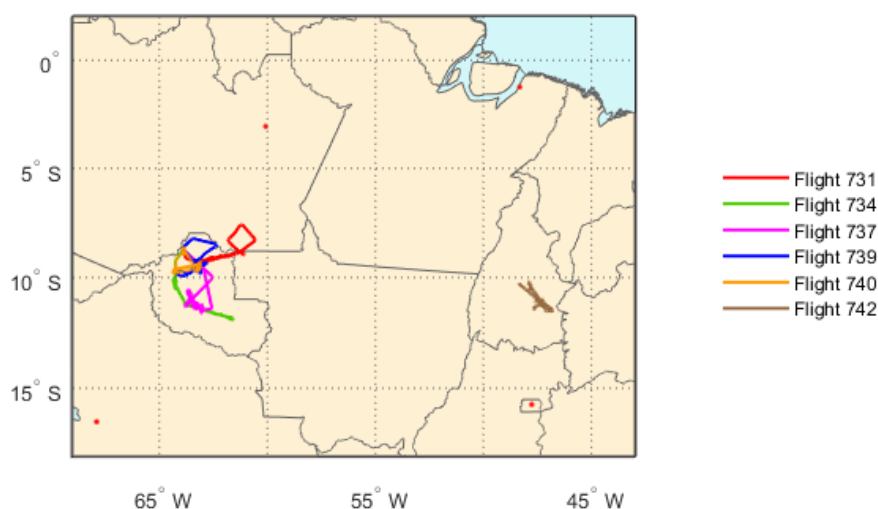
Figure 4.7 Trajectories of the SAMBBA (2012) flights selected to analyze in this study. Flight details are showed in the table 4.2.

Table 4.2 Summary of the SAMBBA flights considered in this study. Latitudes and longitudes are related to the area in which averaged profiles were extracted from model results (shown in figures 4.10 and 4.11).

SAMBBA phase	Flight number	Date	Takeoff / landing	Latitude	Longitude	Good quality data*
	731	14 Sep	Porto Velho	9.3-8.6º S	63.9-61.5º W	43.1%
Phase 1	734	18 Sep	Porto Velho	11.5-8.7º S	64.3-62.8º W	54.4%
	737	20 Sep	Porto Velho	11.3-8.7º S	63.9-63.0º W	54.8%
	739	23 Sep	Porto Velho	9.5-8.4º S	63.9-62.5º W	61.4%
Phase 2	740	25 Sep	Porto Velho	9.6-8.7º S	64.0-63.5º W	46.7%
	742	27 Sep	Palmas	11.2-10.3º S	48.4-47.2º W	62.0%

Palmas   10.25° S, 48.32° W   (*) Data with good flag.
Porto Velho   8.76° S, 63.90° W

For the six flights, carbon monoxide (Fig. 4.8) and ozone (Fig. 4.9) 5-min averaged observations vary from 40 to 1000 ppb and from 5 to 80 ppb, respectively. At high altitudes (greater than 6 km in Amazonia), flights 731 and 737 showed very low concentrations and variability of CO and O_3. This is because is rare to find Pyro-Cbs with altitudes higher than 5 km and, commonly, all the fire emissions are distributed in the lower and middle troposphere. The same occurs in the *Cerrado*, at altitudes higher than 4 km. The difference on the limit altitude where pollutants appears in low concentrations could be related to the atmospheric stability observed in each biome. In the *Cerrado* biome,

specifically in the place where the flight 742 took place, very dry conditions were observed during the campaign (Fig. 4.3). This meteorological conditions are not propitious for the development of plumes with higher tops as the observed in the Amazonia, keeping almost all the pollutants in the layers below than 3 km. Rémy et al. (2016) made a climatology of the top and mean injection heights over different regions of the world. Their results show that the typical injection heights observed in the *Cerrado* biome is 2.5 km, in concordance with the plume sampled by the flight 742.

Model results using PRMv0 and the traditional method used in the 3BEM to create emission fluxes, show lower concentrations of carbon monoxide and ozone than the measured by the aircrafts (Figs. 4.8-4.9), especially in the lower troposphere (below 2 km). For flights 731, 739 and 742, this simulation is computing values of CO of the half of the observation, or even less in some parts of the flight 742. The same is observed when analyzing the ozone: the model run is underestimating the concentrations of this gas in all the flights. Differences in ozone range from 10 to 50 ppb below the observation. Differences are greater for the flight 742, representative of the *Cerrado* biome. This lack is due to the scheme used to estimate the biomass burning in the 3BEM model, that is actually underestimating the fire emissions (this is discussed in section 4.6), but also could be due to the version of the PRM itself.

Simulations made with PRMv1.0 and PRMv1.1 use the 3BEM-FRE emission fluxes and show very similar behavior in all six flights, with few difference between them. Both simulations show a good agreement with the observations in high altitudes and they are overestimating the concentrations of CO and O_3 in the middle and lower troposphere. This is not observed in the flights 739 and 740, in which the simulated carbon monoxide concentration is lower than the aircraft measurement (~150 ppb), but the difference is more significant when analyzing the ozone, which is being underestimating by 40 ppb in some cases where the observation is 80 ppb. This results could suggest: (i) the 3BEM-FRE is overestimating the biomass burning emission fluxes, and/or (ii) the computation of the plume injection heights by the PRM versions is not accurate.
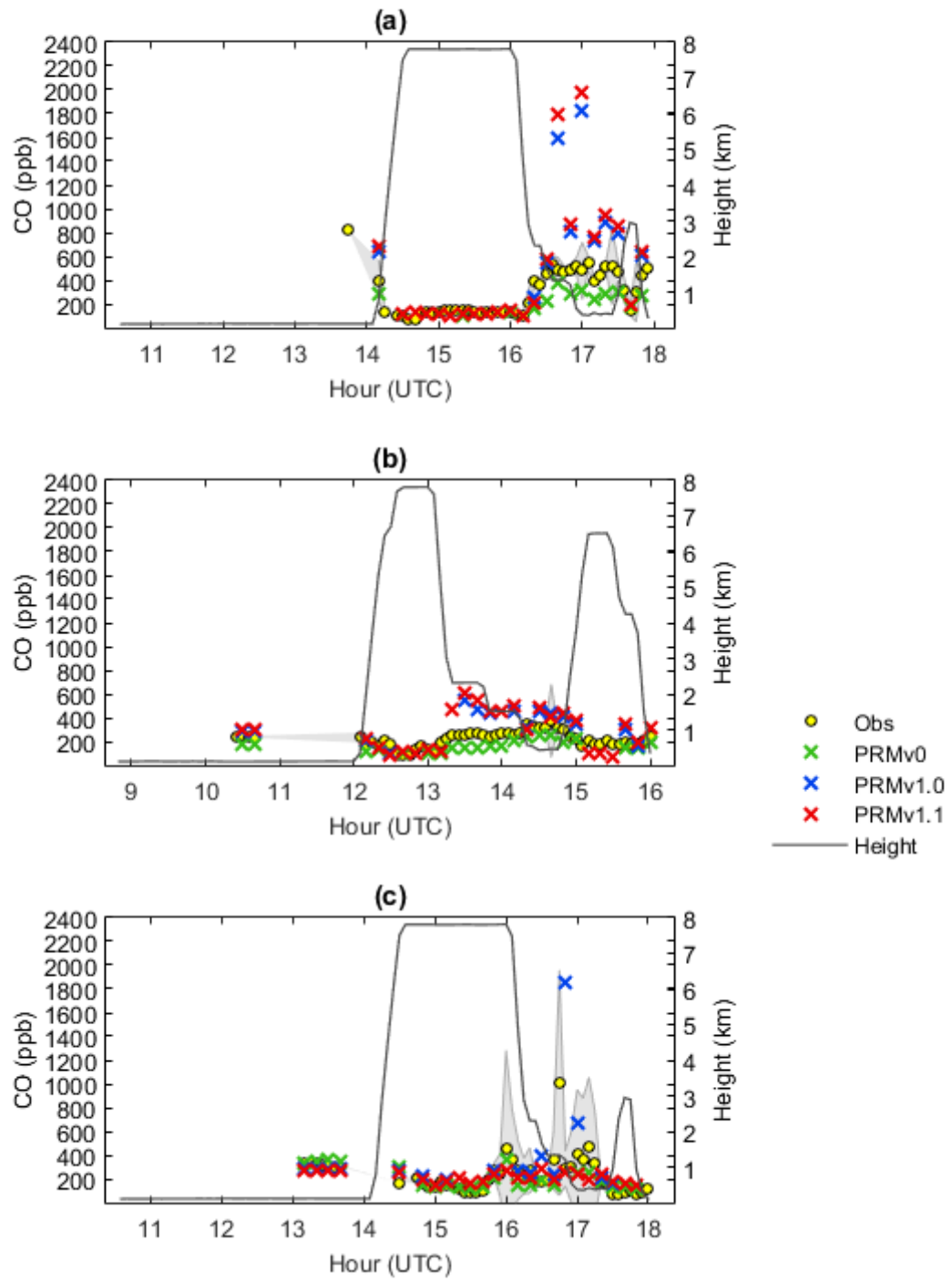
Figure 4.8 Carbon monoxide concentrations (ppb) measured by the flights (a) 731 on 14 Sep. 2012, (b) 734 on 18 Sep. 2012, (c) 737 on 20 Sep. 2012, (d) 739 on 23 Sep. 2012, (e) 740 on 25 Sep. 2012 and (f) 742 on 27 Sep. 2012 of the SAMBBA campaign (yellow circles). Crosses represent the model results using the three versions of the Plume Rise Model (see legend). Standard deviation of the observations is shown as the gray area and flight altitude is shown in the black line.

Figure 4.9 Ozone concentrations (ppb) measured by the flights (a) 731 on 14 Sep. 2012, (b) 734 on 18 Sep. 2012, (c) 737 on 20 Sep. 2012, (d) 739 on 23 Sep. 2012, (e) 740 on 25 Sep. 2012 and (f) 742 on 27 Sep. 2012 of the SAMBBA campaign (yellow circles). Crosses represent the model results using the three versions of the Plume Rise Model (see legend). Standard deviation of the observations is shown as the gray area and flight altitude is shown in the black line.

4.6.   Vertical analysis of SAMBBA flights

The previous analysis did not allow to determine whether the new developments on the 3BEM and PRM models are simulating a realistic vertical structure of the fire emissions. To do this, vertical profiles of observed and simulated CO and O_3 for each flight are shown in figures 4.10 and 4.11. Averaged observations vary in a range of 100-650 ppb of carbon monoxide and from 0-80 ppb of ozone. Variations are low (±15 ppb) for the case of ozone. Carbon monoxide variations are up to ±600 ppb (flights 737 and 742). These higher standard deviations observed for the case of carbon monoxide are observed, mainly, in the lower and middle troposphere, and may be a sign of the plume injection height.

In general terms, the simulation PRMv0 shows lower concentrations of CO and O3 than the flights measurements. However, for the flight 737, this simulation shows a good agreement with the observations of both carbon monoxide and ozone (Fig. 4.10c and Fig. 4.11c). In fact, for flights 731 and 734, this model run simulates both variables better than the other simulations. This could be due to the different emission fluxes used in each run.

Simulations PRMv1.0 and PRMv1.1 show very similar results between them for both carbon monoxide and ozone. Both runs simulate very well the carbon monoxide at altitudes higher than 4 km, but show some lack from the observation in the lower troposphere. This happen on flights of the phase 1 of the campaign (731, 734, 737), where the model is overestimating the concentrations of CO. This is more evident for the flight 731, where the model simulations are showing CO concentrations higher than 1000 ppb near the surface, but the observations are below 600 ppb. During phase 2 of the SAMBBA campaign, models runs show a very good agreement with the measurements made by the aircrafts. In the other hand, these simulations show some difficulty to reproduce the vertical profiles of ozone in all six flights. In some cases, the simulations overestimate or underestimate the observations and this is observed in the whole troposphere from surface to 8 km. The cause
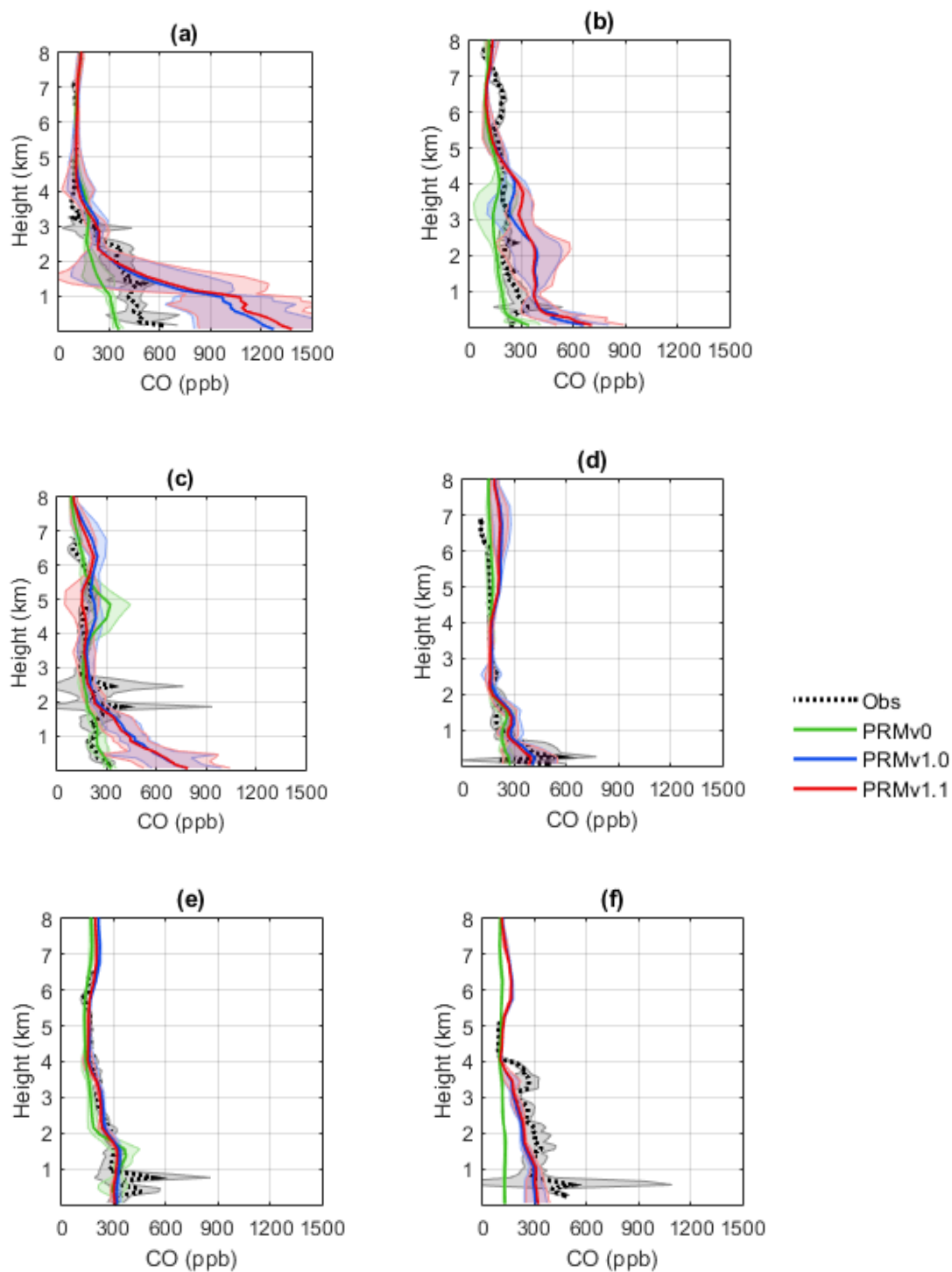
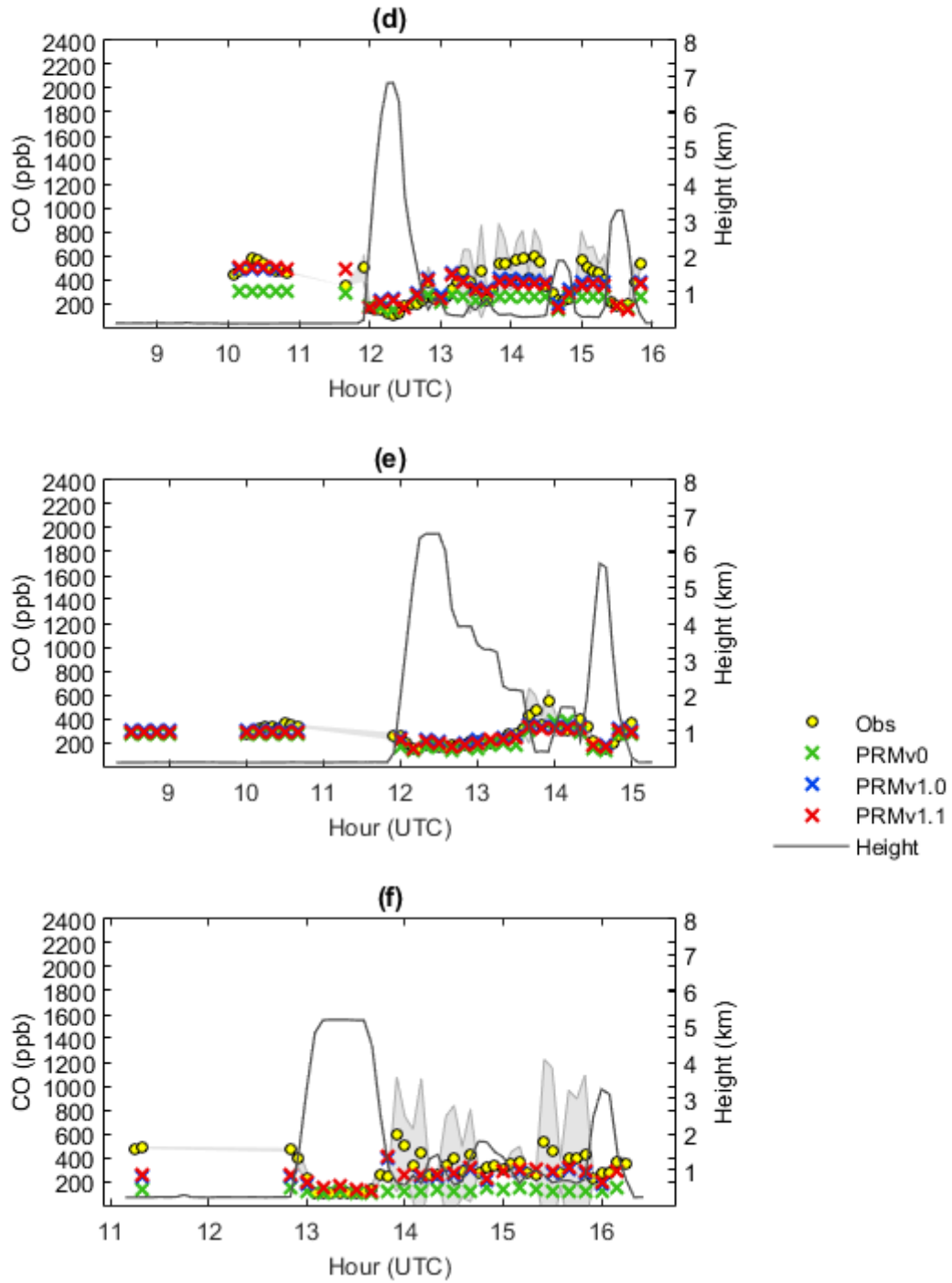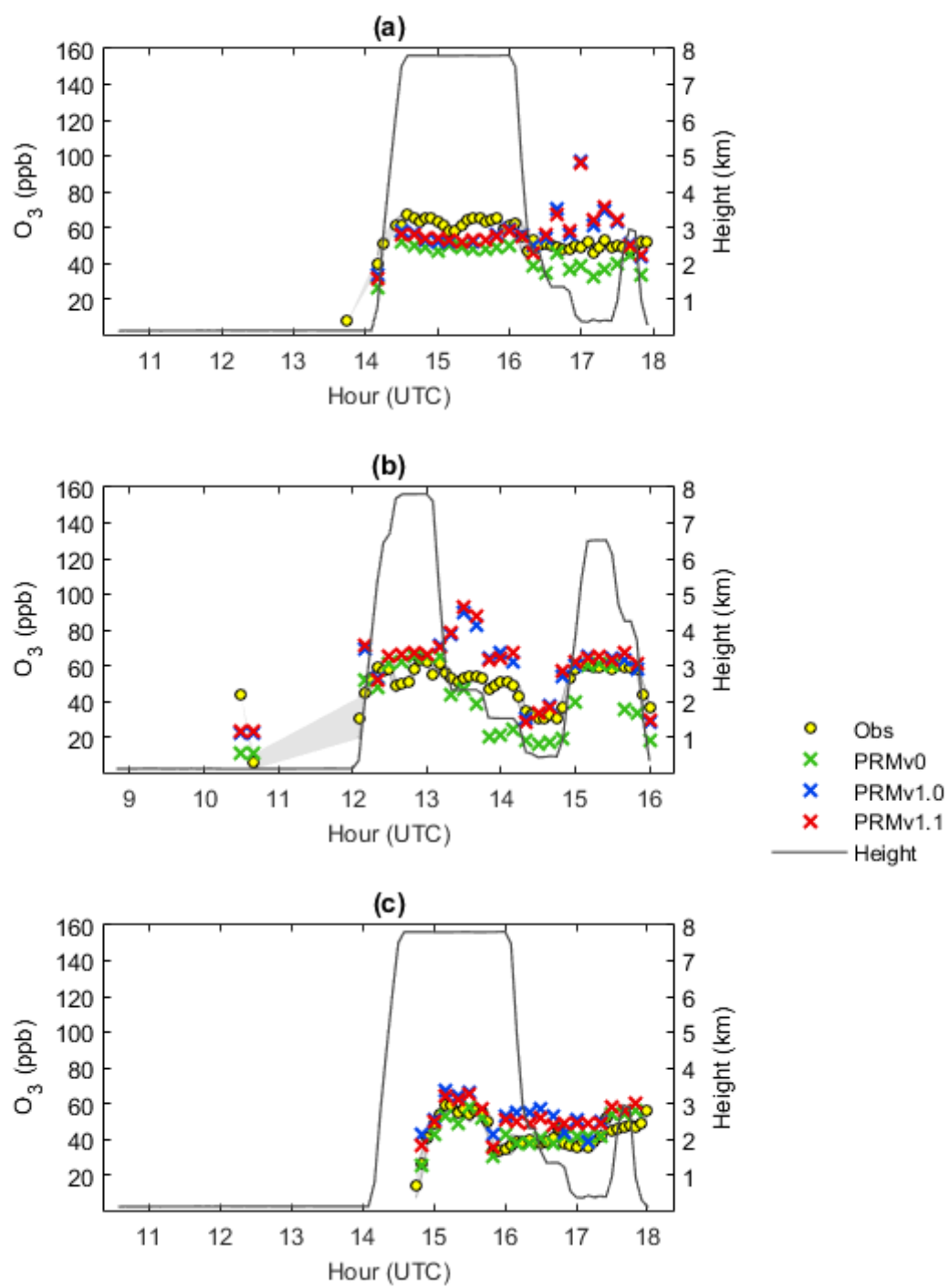**Figure 4.10** Area-averaged vertical profiles of carbon monoxide (ppb) measured by the flights (a) 731 on 14 Sep. 2012, (b) 734 on 18 Sep. 2012, (c) 737 on 20 Sep. 2012, (d) 739 on 23 Sep. 2012, (e) 740 on 25 Sep. 2012 and (f) 742 on 27 Sep. 2012 of the SAMBBA campaign (black dots) and model results using the three versions of the Plume Rise Model (see legend). Shaded areas represent the standard deviation.

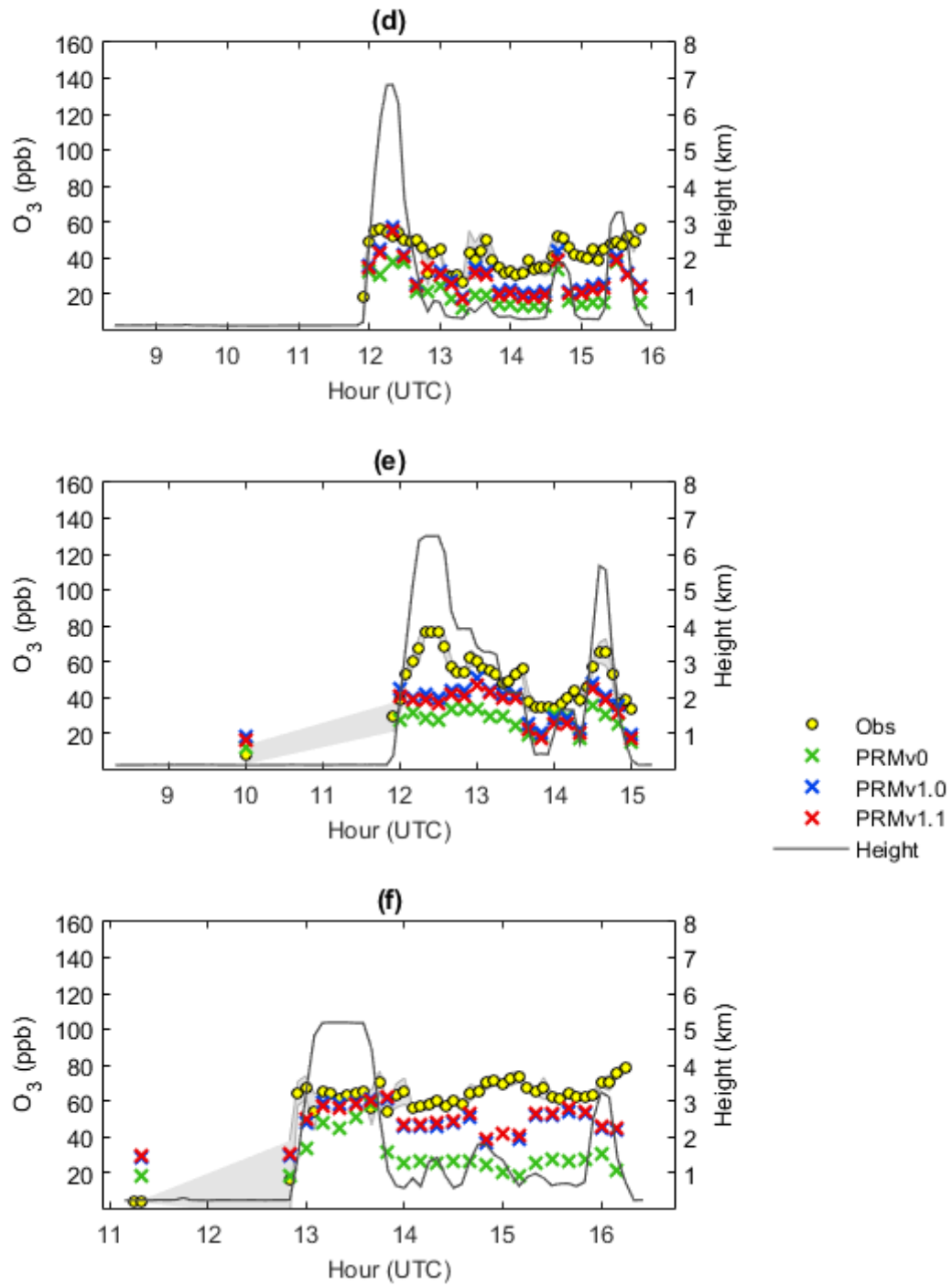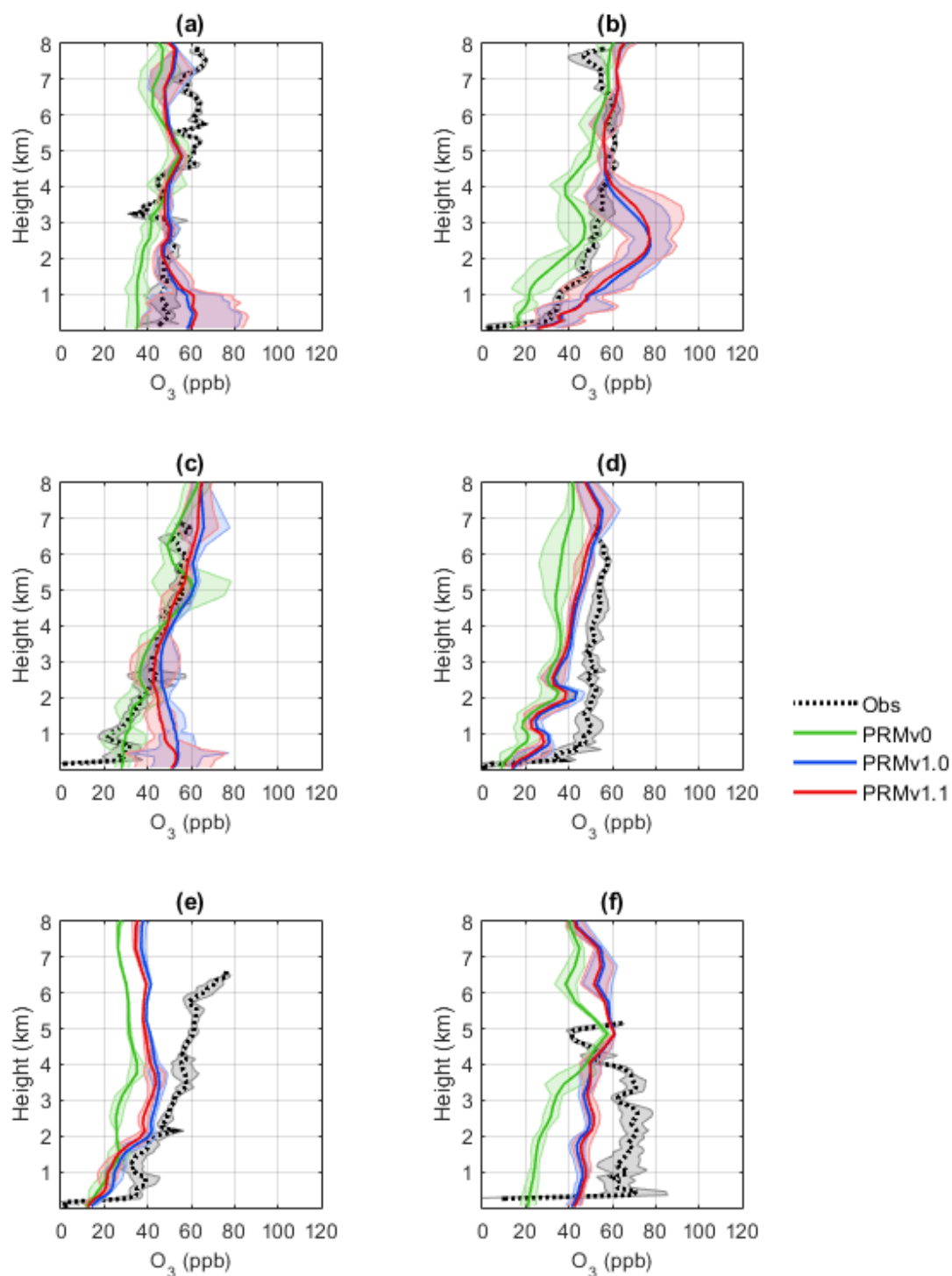**Figure 4.11** Area-averaged vertical profiles of ozone (ppb) measured by the flights (a) 731 on 14 Sep. 2012, (b) 734 on 18 Sep. 2012, (c) 737 on 20 Sep. 2012, (d) 739 on 23 Sep. 2012, (e) 740 on 25 Sep. 2012 and (f) 742 on 27 Sep. 2012 of the SAMBBA campaign (black dots) and model results using the three versions of the Plume Rise Model (see legend). Shaded areas represent the standard deviation.

of this can be several reasons. One of them is the complexity of the formation of the tropospheric ozone, which depends on several factors, such as the relation of nitrogen oxide and nitrogen dioxide, the solar radiation that could be attenuated by the amount of aerosols in the atmosphere, and other compounds. If one of more of this factors is being unbalanced in the model, the ozone production will be altered. In this case, it is necessary to make an analysis of the emission fluxes used in this simulations.

It is important to mention, that the results exposed in this subsection are averaged in an area and in altitude. Consequently, errors could be introduced in the comparison between the observations and the simulations, but the valid data of the flights does not allow to apply a better method to analyze the vertical structure of those gases.

4.7. Horizontal distribution of fire emissions

Figure 4.12 shows the averaged aerosol optical depth at 550 nm (AOD 550) measurements made by MODIS Terra and Aqua satellites, as well as the model results of the three simulations, for the two phases of the SAMBBA campaign. Remote sensing observations show a defined area centered in the Brazilian state of Mato Grosso (15º S-53º W) during the phase 1 of the campaign, with AOD magnitudes higher than 0.5. Also, high values of AOD are observed to the south, passing by Paraguay and southern Brazil, due to the low level jet, which transports the fire emissions away from their source. Also a considerable amount of aerosols is observed in the east side of the Andes range, near latitude 10º S, due to strong trade winds, that even cross the range, showing an AOD up to 0.4 offshore Peru. During phase 2, AOD magnitudes are lower than in phase 1, with a maximum of 0.8 in southern Pará state (Brazil, 7º S-50º W). The both secondary maximum due to the low level jet and the trade winds can also be recognized, but in a magnitude much lower than during the phase 1. This decrease in the concentration of aerosols in the atmosphere is mainly due to the wet removal process, that it stronger in the phase 2, because is the beginning of the wet season in southern Amazonia.
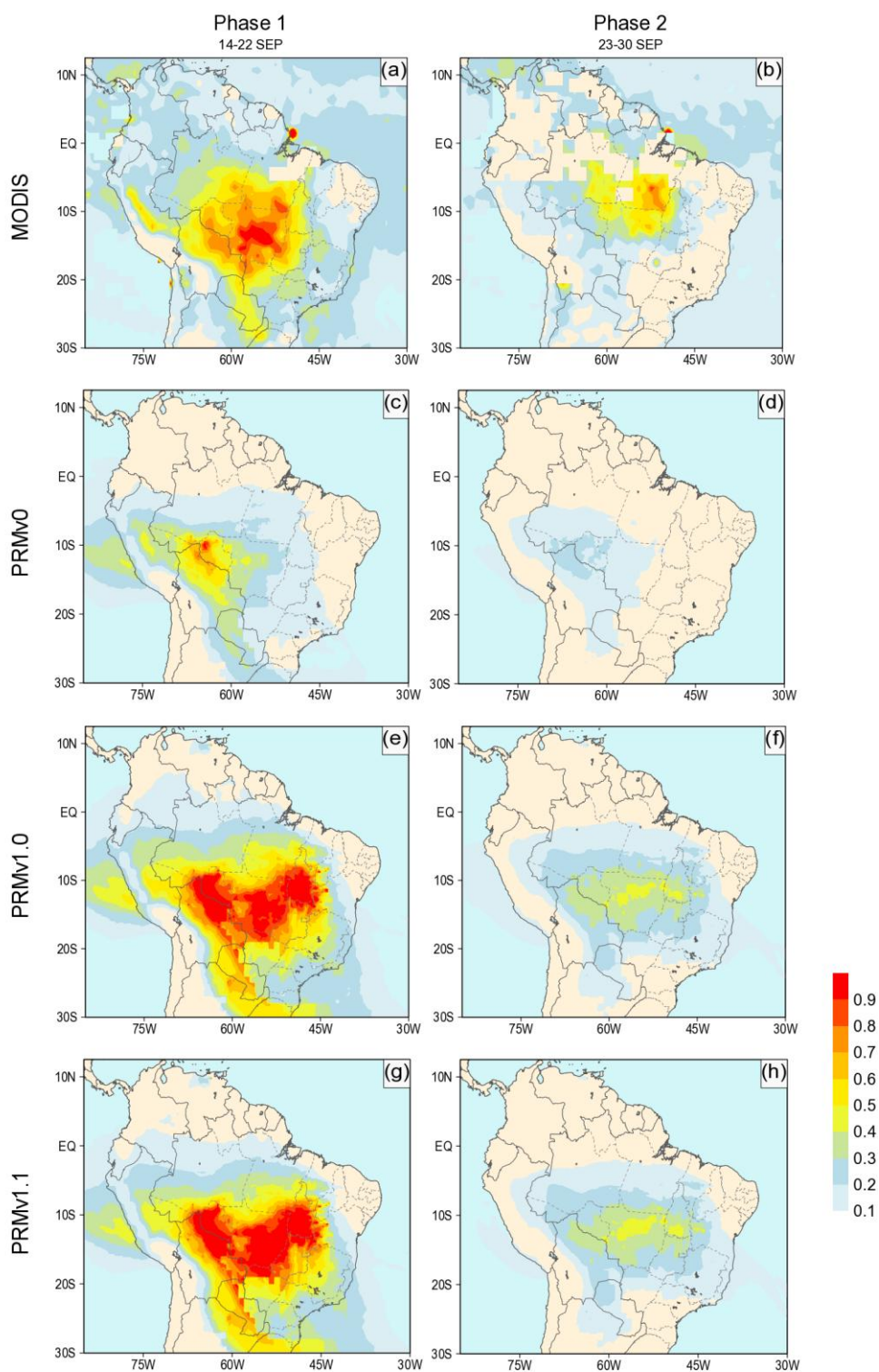
Figure 4.12 Averaged aerosol optical depth at 550 nm in the column during phase 1 (left panels) and phase 2 (right panels) of the SAMBBA campaign (2012). Panels (a) and (b) show the MODIS measurements onboard the Aqua and Terra satellites. Panels (c)-(h) show the model results using the three different versions of the Plume Rise Model.

Simulation PRMv0, which uses the traditional 3BEM formulation to generate the daily biomass burning emissions, is underestimating the MODIS observations in both phases. In addition, the center of the aerosols is showed westward, in the boundary between Brazil and Bolivia, covering a smaller area with AOD values of 0.5, during phase 1, and AOD values below 0.3 during phase 2. This proofs that the 3BEM emissions used in this simulation are not accurate to represent biomass burning emissions during the dry season of the Amazonia. Nevertheless, BRAMS model simulated with success the circulation patterns exposed in the previous paragraph.

Simulations PRMv1.0 and PRMv1.1 show similar behavior since they both used the 3BEM-FRE emissions suggested in this study. Both runs overestimate the AOD measurements during phase 1, showing three relative maxima with AODs higher than 0.8 over central South America. In contrast, during phase 2, these simulations underestimate the amount of aerosols in the atmosphere and show them concentrated in central Brazil, surrounding Mato Grosso state (AODs up to 0.6), while observations during this phase are placed further north. The cause of this, could be explained by figure 4.3, which shows that model runs are overestimating the precipitation in the Amazon. Specifically, by the cumulus parameterization used. Thus, the more rainfall, the higher wet removal of pollutants.

Taking into account the above and the previous results, the enhancement factor used to create the fire emissions was modified, passing from 0.75 to 0.525, in order to reduce the emission fluxes computed by the 3BEM model and adjusting it for operational issues. In general, as the simulation PRMv1.1 showed better results than the other simulations when comparing with data from the SAMBBA campaign, we decided to keep only this configuration for the next analysis. To avoid confusions, hereafter, PRMv1.1 will be called as PRM-new, indicating that uses the 3BEM-FRE emissions using the new enhancement factor value.
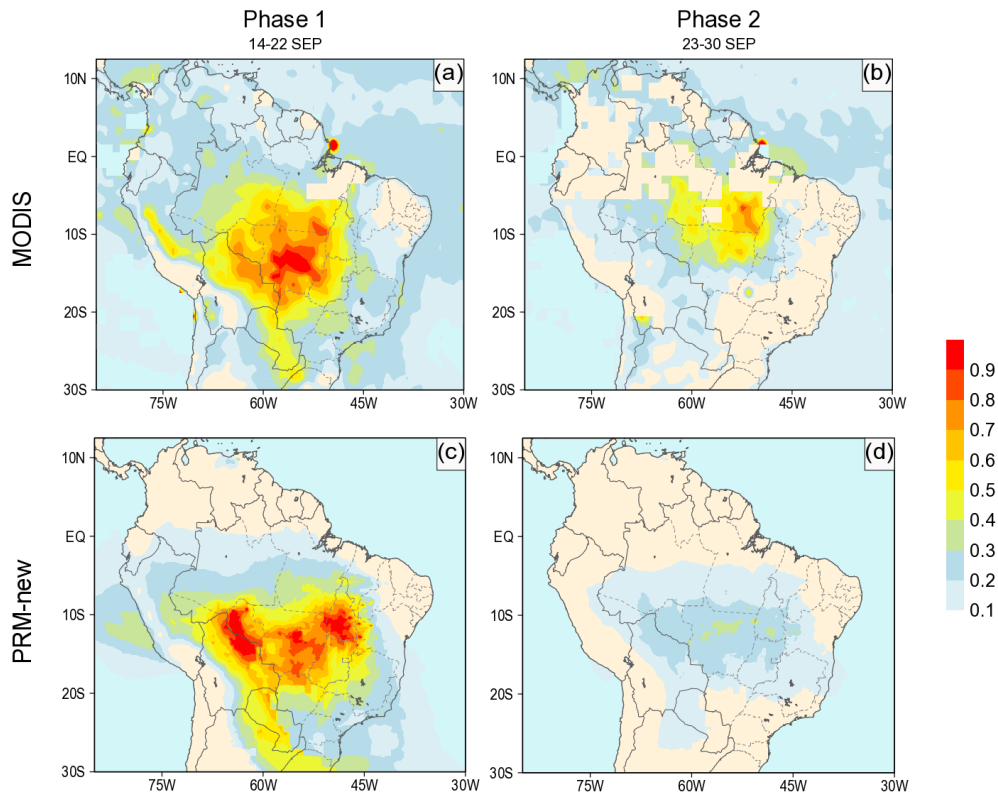
Figure 4.13 Averaged aerosol optical depth at 550 nm in the column during phase 1 (left panels) and phase 2 (right panels) of the SAMBBA campaign (2012). Panels (a) and (b) show the MODIS measurements onboard the Aqua and Terra satellites. Panels (c)-(d) show the model results using the PRMv1.1 ($\beta = 0.88$) and the adjusted 3BEM-FRE emissions.

Figure 4.13 shows the AOD at 550 nm from the simulation PRM-new, as well as the MODIS observations for phases 1 and 2 of the SAMBBA campaign. Note that the simulated distribution of aerosols is in concordance with the past simulations, and are in agreement with the figures 4.4 and 4.5, which expose the fire locations of both phases. However, the simulated AOD 550 values are of the same order of magnitude of the observations during phase 1, ranging from 0.4 to 0.9 in central South America. Though, during phase 2, the problem with reproducing the accurate magnitudes of AOD 550 persists. This suggests that additional improvements are needed onto the 3BEM-FRE model to generate more precise emission fluxes.
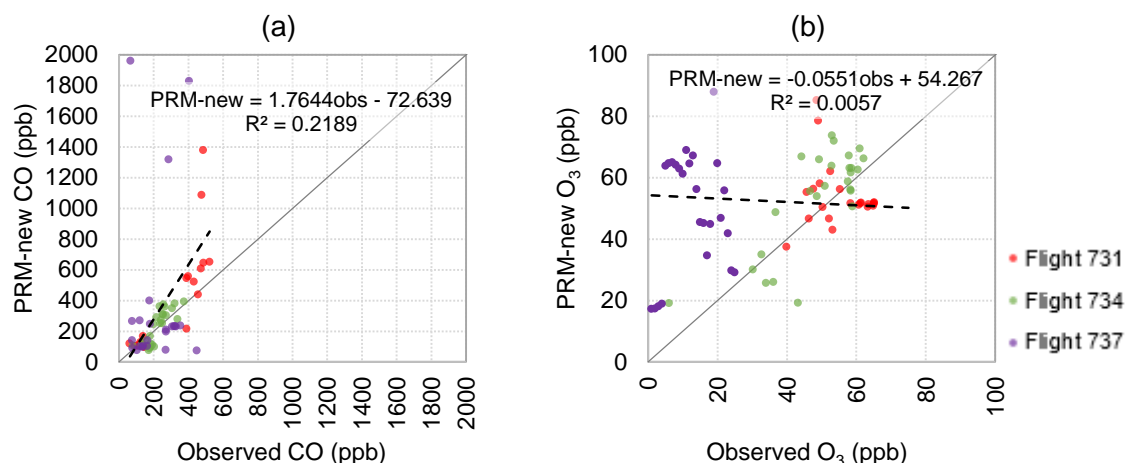
Figure 4.14 Comparison of the results of the simulation PRM-new and SAMBBA flights measurements of (a) carbon monoxide and (b) ozone (ppb) during the Phase 1 of the campaign (14-22 September 2012). For each plot, the best-fit relationship between the observed (obs) and simulated (PRM-new) tracer is shown as the dashed line. In addition, the coefficient of determination (R^2) is informed.
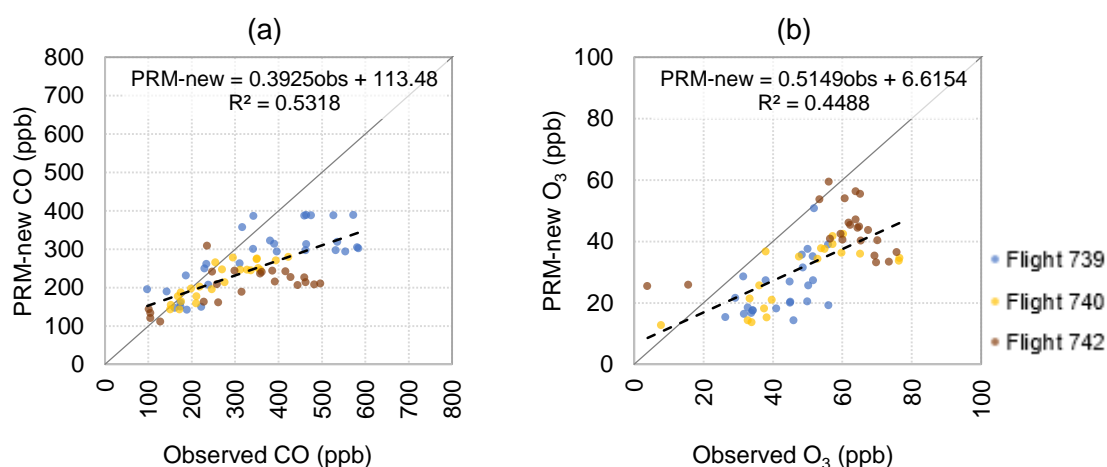
Figure 4.15 Comparison of the results of the simulation PRM-new and SAMBBA flights measurements of (a) carbon monoxide and (b) ozone (ppb) during the Phase 2 of the campaign (23-30 September 2012). For each plot, the best-fit relationship between the observed (obs) and simulated (PRM-new) tracer is shown as the dashed line. In addition, the coefficient of determination (R^2) is informed.

Comparisons of trace gases between the simulation PRM-new and the six SAMBBA flights during phase 1 (Fig. 4.14) and phase 2 (Fig. 4.15) of the campaign, show that the model is overestimating (underestimating) the CO and

O_3 concentrations during the phase 1 (phase 2), in agreement with the figure 4.13, as explained in the previous paragraph. The model is better simulating the structure both variables during the phase 2, showing correlations greater than 0.45. During the two phases of the campaign, the model has a higher skill when simulating carbon monoxide than simulating ozone, regarding in the complexity of ozone formation. Factors as the model spatial resolution used (20 km) can influence in this results, especially because the model grid box represents the mean values of every computed variable and, the flights, made punctual and local measurements that could be hidden by the model grid selected.

4.8. SAMBBA LIDAR measurements analysis

Two flights with LIDAR measurements of aerosol extinction were selected for this analysis, representatives of the phases 1 and 2 of the SAMBBA campaign (Fig. 4.16 and Table 4.3). Flight 733 measures the aerosol emitted by biomass burning in the Amazon forest and, flight 743, measures biomass burning emissions in the *Cerrado* and Amazon forest, covering a greater area.

Both flights show a similar structure, with a moderate magnitude of aerosol extinction, of the order of 150-200 μm^{-1} (Fig. 4.17a,b), between the surface and an upper altitude of 4-5 km, with some localized patches showing greater magnitudes. Flight 733 samples a layer of aerosols in the middle troposphere at 65-66º W coming from the east, caused by the trade winds; and show another separated region of aerosols in the lower troposphere between 66-67º W, caused mainly by local fires. Flight 743 measures four local fires: at 51º, 52.3º, 54.5º and 59.5º W, showing aerosol extinction coefficients greater than 400 μm^{-1}. Uncertainties of both flights are showed in figure 4.17c,d, displaying the highest errors near the surface.

Assuming that carbon monoxide has a behavior similar to aerosol particles, this variable was used to compare against observations in this section. PRM-new simulation was able to reproduce the structures sampled by the flight 733, showing an upper troposphere (higher than 4 km) almost clean of pollutants (Fig. 4.18a). In addition, it reproduces the structure carried out from the east
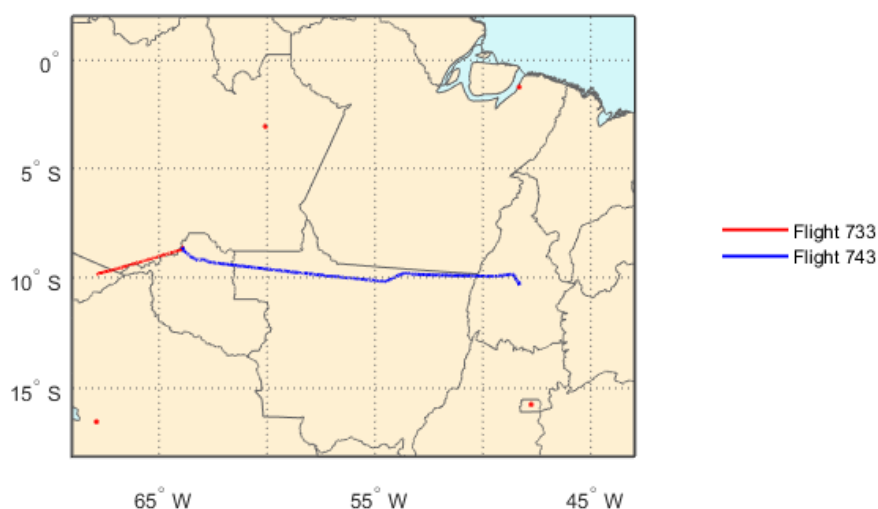
Figure 4.16 Trajectories of the SAMBBA (2012) flights used in this study. Flight details are showed in the table 4.3.

Table 4.3   Summary of the SAMBBA campaign flights used in this study, with the LIDAR instrument onboard the airplanes.

SAMBBA phase	Flight number	Date	Takeoff / landing	Departure	Return	Good quality data*
Phase 1	733	16 Sep	Rio Branco / Porto Velho	12:00	15:55	22.5%
Phase 2	743	27 Sep	Palmas / Porto Velho	18:00	21:30	98.1%

Palmas	10.25° S, 48.32° W
Porto Velho	8.76° S, 63.90° W
Rio Branco	9.98° S, 67.82º W

with the trade winds, showing the higher concentration of CO in that layer (between 350 and 600 ppb). However, the model has some difficulty in the reproduction of the western region with high concentration of aerosols in the lower troposphere. The model is distributing the emissions near the surface.

PRM-new results reproduced some two of the four single fires detected by the flight 743, specifically those located in the *Cerrado* region (at 51º and 52.3º W). Those observed plumes reached the 3 km and the model is showing a great amount of CO at 4 km (related to the fire at 51º W), that is the injection height computed by the PRMv1.1. The fire located at 52.3º W is simulated with an injection height in agreement with the observation at 3 km. Nevertheless, it is important to note that the differences between the model results and the LIDAR
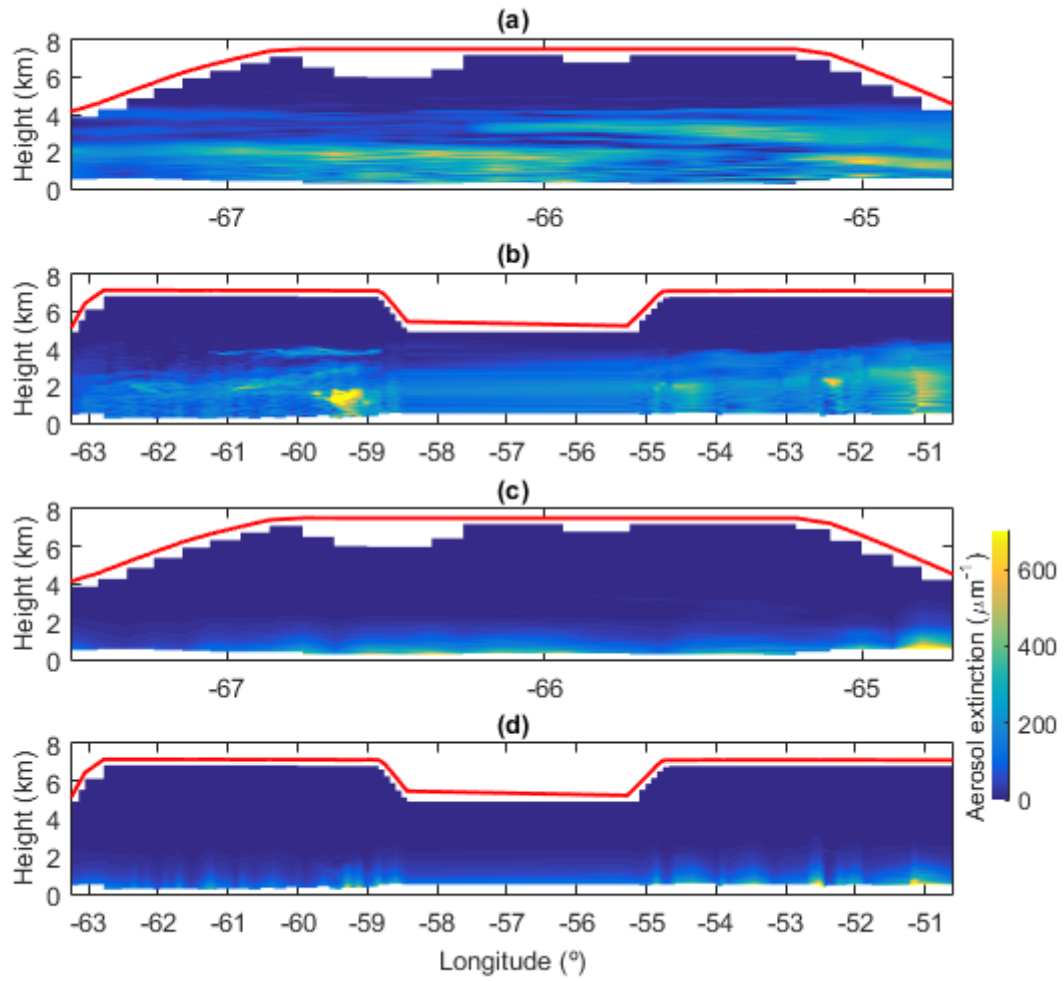
Figure 4.17 Cross sections of aerosol extinction coefficient (µm^{-1}, a and b) and its measurement uncertainty (µm^{-1}, c and d) determined from the LIDAR instrument, for the research flights (a and c) 733 on 16 September 2012 (Phase 1); and (b and d) 743 on 27 September 2012 (Phase 2), with an integration time of 1 min. Red lines indicate the aircraft altitude.

measurements regard to (i) the model spatial resolution used is 20 km, which can attenuate the effect of single fires, since the majority of them are of a size much lower than that, (ii) model output does not include the aerosol extinction variable, which would be the ideal parameter to compare directly with the observations and (iii), model CO cross section was computed as the average of the mean latitude of flight and at the mean time of flight, obviously, this technique could introduce several errors.
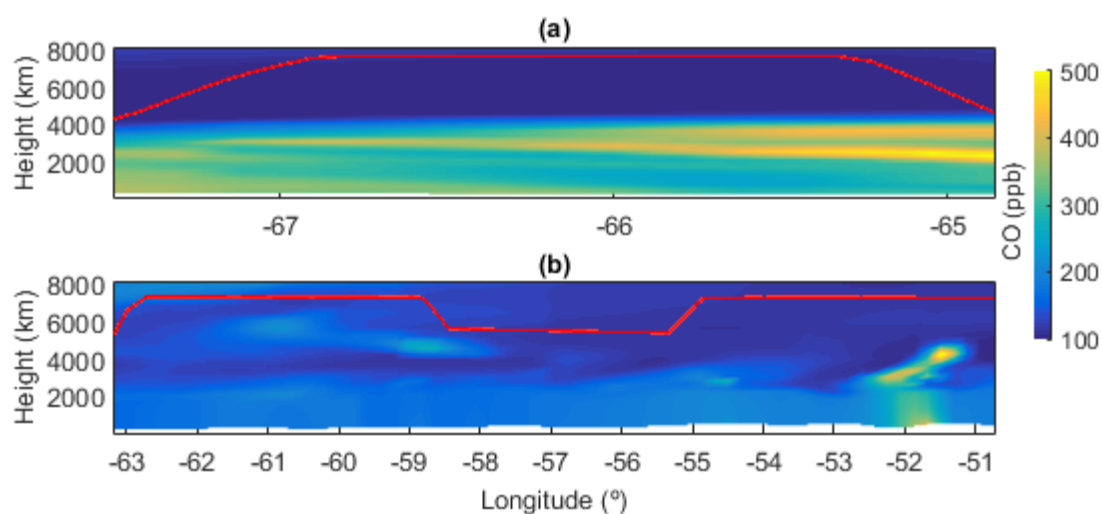
Figure 4.18 Cross sections of averaged carbon monoxide (ppb) simulated with the adjusted 3BEM-FRE emissions and using PRMv1.1 onto the BRAMS model for the flights (a) 733 on 16 September 2012 (phase 1, averaged at latitude 9.3º S); and (b) 743 on 27 September 2012 (phase 2, averaged at latitude 9.6º S). Red lines indicate the aircraft altitude to compare with LIDAR aerosol extinction observations of the figure 4.15.

5   SUMMARY AND CONCLUSIONS

The SAMBBA campaign took place in September 2012 in the southern Amazonia and the Brazilian *Cerrado* regions (savanna like biome), with the aim of measure diverse trace gases and aerosols emitted by the intense biomass burning activity of this region. This study was centered in agreement with this campaign and six of the twenty flights were used to analyze the horizontal and vertical structures of the BRAMS model (version 5.2), by using different versions of the Plume Rise Model embedded into it. In addition, the 3BEM model was modified to include the fire radiative energy, retrieved by remote sensing, to estimate the daily emission fluxes of the biomass burning. Then, two additional flights with LIDAR aerosol extinction measurements were used.

SAMBBA campaign was divided in two phases according to the amount of precipitation over the central South America. Phase 1 (14-22 September 2012) was characterized by dry weather conditions, with accumulates of rainfall of ~30 mm in southern Amazonia. This dry conditions were very favorable for the ignition of big and powerful fires, some of them bigger than 100 ha. In the same way, measurements of fire radiative power (FRP) in units of thousands of MW. The dry-to-wet transition was observed in the phase 2 of the campaign (23-30 September 2012), with accumulates of rain about 70 mm in southern Amazonia, but the *Cerrado* remained dry, with ~10 mm of accumulated precipitation. Thus, detected fires were smaller and weaker in the Amazonia than the observed during the phase 1. In both phases, model results overestimate TRMM rainfall observations. This may be due to the shallow or deep cumulus parameterizations used. It is important to clarify the differences between the TRMM satellite estimations of rainfall when comparing with the BRAMS model results: TRMM has difficulty to "see" the warm clouds in which rains. It was developed to measure the rainfall from deep convection measurements. The precipitation from warm clouds in Amazonia is very frequent, but there is not exist an estimated percentage of how much of the total precipitation is due to this kind of clouds to compare with the model.

The six flights studied were selected according to their aims of measurements and quality of the data. In general terms, BRAMS runs made with the original version of the Plume Rise Model (PRMv0) and the fire emission fluxes created with the 3BEM model, are underestimating the concentration of both carbon monoxide and ozone in the lower and middle troposphere. The cause of this regards on the 3BEM emissions, made with the traditional formulation of it. This is confirmed by the figure 4.12, which shows AOD 550 measurements by MODIS Terra and Aqua satellites and the model results, as discussed in section 4.7. In contrast, in the upper troposphere (altitudes higher than 6 km), the model shows a good concordance with the observations.

Model runs made with the new version of the Plume Rise Model (PRMv1.0 and PRMv1.1) and using fire emission fluxes from the 3BEM-FRE model, show few differences between them and greater trace gases concentrations than with the PRMv0 simulation are observed. In some cases, especially in the lower and middle troposphere, they are overestimating the gases concentrations. This suggested that the 3BEM-FRE emissions are being overestimated. Hence, a new enhancement factor to convert from FRE to emission fluxes in the 3BEM-FRE was set, passing from 0.75 to 0.525. New biomass burning emissions were lower than the previous and higher than the traditional 3BEM emissions (Fig. 4.13), showing a good fit during phase 1 of the campaign, but underestimating the aerosols during the phase 2. This proposes that additional improvements than the made in this study are needed to improve the 3BEM-FRE performance, but also, the explanation of the lack between the MODIS observations of AOD at 550 nm can be explained by the overestimation in the rainfall, that is higher during phase 2, increasing the wet removal processes of pollutants.

At this point, a new simulation was added using the PRMv1.1 and the new 3BEM-FRE emissions described in the preceding paragraph. This simulation showed better results than the other simulations when analyzing the six SAMBBA flights selected. Thus, the 3BEM-FRE model using the new enhancement factor is better for simulating the distribution of trace gases during September 2012, than the traditional formulation of it.

Regarding to the two flights with LIDAR aerosol extinction measurements, the model was able to reproduce some of the structures observed, principally during the phase 1 in southern Amazonia (flight 733), but with some difficulty during the phase 2. Indeed, caused by the underestimation of the fire emissions in this phase of the campaign in this region. In the other hand, during phase 2, the model had success in the *Cerrado* region, showing well reproduced injection heights of two single fires observed. One of them had an observed injection height of 3 km and the model simulated a height of 4 km. The other fire was simulated with success with an injection height of 3 km. Fires observed in the Amazonia were not well reproduced. In general terms, the model has agreement with the observations showing that all pollutants are concentrated below 4 km during both phases of the campaign.

Summarizing, the PRM and 3BEM developments presented here showed better results than the original versions of them when simulating the fire emissions and plumes in South America during the SAMBBA campaign. The inclusion of remote sensing data for the initialization of the models improved their performance, showing correlations around 0.5 when comparing with observations. This is because of the fires are treated as individual fires avoiding errors introduced by generalization according to the biomes.

Simulations made with the new versions of the PRM and using the 3BEM-FRE, showed good results of the distribution and concentration of pollutants emitted by biomass burning in the middle and upper troposphere, but in some cases, with difficulty in the lower atmosphere (overestimating by ~20-30%). This is observed, principally, when analyzing ozone profiles. Due to the complexity of the formation of it in the troposphere, it is comprehensive that the model shows errors.

Differences between the observations and the model outputs, can be due to the complex paths of the aircrafts in the altitude and the horizontal and it is important to consider that the model spatial resolution (20 km horizontal, 45 vertical levels) represents the mean of the grid, and not the value observed in that point. This introduces errors when comparing with punctual observations as

of the SAMBBA campaign flights. Vertical resolution of the model is more complex. It is stretched near the surface, to have a good resolution in the turbulence of the planetary boundary layer and it goes with a gross resolution as the altitude increases. This reasons make difficult to compare with the observational data and maybe may require runs with a finer resolution than that.

Additional validations of the models used are needed. Some of them, regarding on the validation for other dates and regions of the globe, comparing with wide-range observational datasets. In addition, improvements of the physics of the model can be made in both PRM and 3BEM-FRE models. Specifically, improving the entrainment scheme of the PRM, which is currently based on the natural convection of clouds to develop the fire plumes and, as the temperatures of fires are several times greater than the observed in natural convection, the PRM make an overestimation of the plume injection heights. Similarly, improvements in the algorithms used to filter the fire data retrieved by remote sensing are needed, regarding to reduce the errors of measure and estimation of fire size and FRP that then will be used by both models initialization.

REFERENCES

ANDREAE, M. Biomass burning: Its history, use and distribution and its impact on environmental quality and global climate. In: LEVINE, J. S. (Ed.). **Global biomass burning:** atmospheric, climatic and biospheric implications. Cambridge, Mass.: MIT Press, 1991. p. 3–21.

ANDREAE, M. et al. Transport of biomass burning smoke to the upper troposphere by deep convection in the equatorial region. **Geophys. Res.** v. 28, n. 6, p. 951–954, 2001.

ANDREAE, M. et al. Carbon monoxide and related trace gases and aerosols over the Amazon Basin during the wet and dry seasons. **Atmospheric …**, 2012.

ANDREAE, M.; MERLET, P. Emission of trace gases and aerosols from biomass burning. **Global biogeochemical cycles**, v. 15, n. 4, p. 955–966, 2001.

ANDREAE, M. O. The dark side of aerosols. **Nature**, v. 409, n. 6821, p. 671–2, 8 fev. 2001.

ANDREAE, M. O. et al. Smoking rain clouds over the Amazon. **Science (New York, N.Y.)**, v. 303, n. 5662, p. 1337–42, 27 fev. 2004.

ARCHER-NICHOLLS, S. et al. Characterising Brazilian biomass burning emissions using WRF-Chem with MOSAIC sectional aerosol. **Geoscientific Model Development Discussions**, v. 7, n. 5, p. 6061–6131, 17 set. 2014.

BELA, M. M. et al. Ozone production and transport over the Amazon Basin during the dry-to-wet and wet-to-dry transition seasons. **Atmospheric Chemistry and Physics**, v. 15, n. 2, p. 757–782, 21 jan. 2015.

BERGE, E. Coupling of wet scavenging of sulphur to clouds in a numerical weather prediction model. **Tellus B**, v. 45, n. 1, p. 1–22, fev. 1993.

BRASSEUR, G.; HAUGLUSTAINE, D. MOZART, a global chemical transport model for ozone and related chemical tracers: 1. Model description. **Journal of Geophysical Research** v. 103, n. D21, p. 28265–28289, 1998.

BRITO, J. et al. Ground based aerosol characterization during the South American Biomass Burning Analysis (SAMBBA) field experiment. **Atmospheric Chemistry and Physics Discussions**, v. 14, n. 8, p. 12279–12322, 2014.

CHATFIELD, R. B. et al. A general model of how fire emissions and chemistry produce African/oceanic plumes (O 3 , CO, PAN, smoke) in TRACE A. **Journal of Geophysical Research**, v. 101, n. D19, p. 24279, 1 out. 1996.

CHATFIELD, R.; CRUTZEN, P. Sulfur dioxide in remote oceanic air: Cloud transport of reactive precursors. **Journal of Geophysical Research,**v. 89, n. D5, p. 7111–7132, 1984.

CHATFIELD, R.; DELANY, A. Convection links biomass burning to increased tropical ozone: However, models will tend to overpredict O3. **Journal of Geophysical Research** v 95, n. D11, p. 18473–18488, 1990.

CHATFIELD, R.; GUO, Z.; SACHSE, G. The subtropical global plume in the Pacific Exploratory Mission- Tropics A (PEM- Tropics A), PEM- Tropics B, and the Global Atmospheric Sampling Program. **Journal of Geophysical Research**, v. 107, n. D16, 2002. 10.1029/2001JD000497.

CHIN, M. et al. Atmospheric sulfur cycle simulated in the global model GOCART: Model description and global properties. **Journal of Geophysical Research**, v. 105, n. D20, p. 24671, 1 out. 2000.

COLARCO, P. R. Transport of smoke from Canadian forest fires to the surface near Washington, D.C.: Injection height, entrainment, and optical properties. **Journal of Geophysical Research**, v. 109, n. D6, p. D06203, 2004.

COTTON, W. R.; PIELKE, R. A. **Human impacts on weather and climate**. [S.l.] Cambridge University Press, 2007.

DOZIER, J. A method for satellite identification of surface temperature fields of subpixel resolution. **Remote sensing of Environment**, v.11, p. 221-229, 1981.

DUNCAN, B. N. Interannual and seasonal variability of biomass burning emissions constrained by satellite observations. **Journal of Geophysical Research**, v. 108, n. D2, p. 4100, 2003.

FREEBORN, P.; WOOSTER, M.; HAO, W. Relationships between energy release, fuel mass loss, and trace gas and aerosol emissions during laboratory biomass fires. **Journal of Geophysical Research**, v. 113, n, D1, 2008.

FREITAS, S.; DIAS, M.; DIAS, P. Modeling the convective transport of trace gases by deep and moist convection. **Hybrid Methods in Engineering**, v. 3, p. 317–330, 2000a.

FREITAS, S.; DIAS, M. S.; DIAS, P. S. A convective kinematic trajectory technique for low-resolution atmospheric models. **Journal of Geophysical Research**, v. 105, n. D19, p. 24375–24386, 2000b.

FREITAS, S. R. et al. Monitoring the transport of biomass burning emissions in South America. **Environmental Fluid Mechanics**, v. 5, n. 1-2, p. 135–167, 2005.

FREITAS, S. R. et al. Including the sub-grid scale plume rise of vegetation fires in low resolution atmospheric transport models. **Atmospheric Chemistry and Physics Discussions**, v. 6, n. 6, p. 11521–11559, 2006.

FREITAS, S. R. et al. The Coupled Aerosol and Tracer Transport model to the Brazilian developments on the Regional Atmospheric Modeling System (CATT-BRAMS) – Part 1: Model description and evaluation. **Atmospheric Chemistry and Physics**, v. 9, n. 8, p. 2843–2861, 2009.

FREITAS, S. R. et al. Technical note: sensitivity of 1-D smoke plume rise models to the inclusion of environmental wind drag. **Atmospheric Chemistry**

and Physics Discussions, v. 9, n. 4, p. 14713–14733, 2010.

FREITAS, S. R. et al. PREP-CHEM-SRC - 1.0: A preprocessor of trace gas and aerosol emission fields for regional and global atmospheric chemistry models. **Geoscientific Model Development**, v. 4, n. 2, p. 419–433, 2011.

FREITAS, S. R. et al. The Brazilian developments on the Regional Atmospheric Modeling System (BRAMS 5.2): an integrated environmental model tuned for tropical areas. **Geoscientific Model Development Discussions**, v. 0, p. 1–55, 7 jun. 2016.

FREITAS, S. R.; LONGO, K. M.; ANDREAE, M. O. Impact of including the plume rise of vegetation fires in numerical simulations of associated atmospheric pollutants. **Geophysical Research Letters**, v. 33, n. 17, p. L17808, 2006.

FROMM, M. et al. The untold story of pyrocumulonimbus. **Bulletin of the American Meteorological Society**, v. 91, n. september, p. 1193–1209, 2010.

FROMM, M. D.; SERVRANCKX, R. Transport of forest fire smoke above the tropopause by supercell convection. **Geophysical Research Letters**, v. 30, n. 10, p. n/a–n/a, 15 maio 2003.

GALANTER, M.; LEVY, H. Impacts of biomass burning on tropospheric CO, NO x, and O3. **Journal of Geophysical Research**, v. 105, n. D5, p. 6633-6653, 2000.

GEAVERD, R.; FREITAS, S. Estimativa operacional da umidade do solo para iniciação de modelos de previsão numérica da atmosfera. Parte 1: Descrição da metodologia e. **Revista Brasileira de Meteorologia**, v. 21. n. 3, 2006.

GIGLIO, L. et al. An enhanced contextual fire detection algorithm for MODIS. **Remote Sensing of Environment**, v. 87, n. 2-3, p. 273–282, out. 2003.

GRELL, G. et al. Fully coupled "online" chemistry within the WRF model. **Atmospheric …**, v. 39, p. 6957–6975, 2005.

GRELL, G. et al. Inclusion of biomass burning in WRF-Chem: impact of wildfires on weather forecasts. **Atmospheric Chemistry and Physics**, v. 11, n. 11, p. 5289–5303, 2011.

GRELL, G.; DVNYI, D. A generalized approach to parameterizing convection combining ensemble and data assimilation techniques. **Geophysical Research Letters**, v. 29, n. 14, 2002. DOI: 10.1029/2002GL015311.

GRELL, G.; EMEIS, S.; STOCKWELL, W. Application of a multiscale, coupled MM5/chemistry model to the complex terrain of the VOTALP valley campaign. **Atmospheric Environment,** v. 34, n. 9, 2000, p, 1435–1453, 2000.

HART, W.; SPINFAIIAE, J. Correlation between smoke and (ropospheric ozone concentration in Cuiabá during Smoke. Clouds, and Radiation-Brazil (SCAR-B). **Journal of Geophysical,** v. 104, n. D10, p. 12113–12129, 27 May , 1999.

HOROWITZ, L. W. et al. A global simulation of tropospheric ozone and related tracers: description and evaluation of MOZART, version 2. **Journal of Geophysical Research: Atmospheres**, v. 108, n. D24, p. n/a–n/a, 27 dez. 2003.

HUFFMAN, G. J. et al. Global precipitation at one-degree daily resolution from multisatellite observations. **Journal of Hydrometeorology**, v. 2, p. 36-50, 2001. http://dx.doi.org/10.1175/1525-7541(2001)002<0036:GPAODD>2.0.CO;2, 2001.

JAFFE, D. A.; WIGDER, N. L. Ozone production from wildfires: a critical review. **Atmospheric Environment**, v. 51, p. 1–10, maio 2012.

JUSTICE, C.; VERMOTE, E.; TOWNSHEND, J. The Moderate Resolution Imaging Spectroradiometer (MODIS): Land remote sensing for global change research. **IEEE Transactions on Geoscience and Remote Sensing,** v. 36,n. 4, 1228 - 1249, 1998.

KAHN, R. et al. Aerosol source plume physical characteristics from space-based multiangle imaging. **Journal of Geophysical Research,** v. 112, n. D11,16 June 2007.

KAHN, R. et al. Wildfire smoke injection heights: Two perspectives from space. **Journal of Geophysical Research,** v. 35, n. 4, Febr 2008.

KARL, T.; GUENTHER, A.; YOKELSON, R. The tropical forest and fire emissions experiment: Emission, chemistry, and transport of biogenic volatile organic compounds in the lower atmosphere over Amazonia. **Journal of Geophysical Research**, v. 112, n. D18, 27 Sept 2007.

KAUFMAN, Y. Remote sensing of direct and indirect aerosol forcing. **Aerosol forcing of climate**, 1995.

KAUFMAN, Y. J.; TANRÉ, D. **Algorithm for remote sensing of tropospheric aerosol from MODIS**. NASA MODIS Algorithm Theoretical**.** Nasa Goddard Space Flight Center, 1998. 85p.

KAUFMAN, Y.; JUSTICE, C.; FLYNN, L. Potential global fire monitoring from EOS-MODIS. **Journal of Geophysical Research** , v. 103, n. D24, p. 32215–32238, 27 Dec 1998.

KAUFMAN, Y.; KLEIDMAN, R. SCAR-B fires in the tropics- properties and remote sensing from EOS-MODIS. **Journal of Geophysical Research**, v. 103, n. D24, p. 31955–31968, 27 Dec. 1998.

KAUFMAN, Y.; REMER, L.; OTTMAR, R. Relationship between remotely sensed fire intensity and rate of emission of smoke: SCAR-C experiment. In: LEVINE, J. (Ed.), **Global biomass burning.** MA: MIT Press, 1996. p. 685-696, 1996. KESSLER, E. On the distribution and continuity of water substance in atmospheric circulation. **Atmospheric Research**, v. 38, n. 1, p.109-145, Sep. 1995.Reads DOI: 10.1016/0169-8095(94)00090-Z.

LATHAM, D. **PLUMP**: A one-dimensional plume predictor and cloud model for fire and smoke managers. Ft. Collins, CO: USDA Forest Service, Intermountain

Research Station, 1994. **(**General Technical Report INT-GTR-314).

LOBERT, J.; WARNATZ, J. Emissions from the combustion process in vegetation. In: CRUTZEN, P. J.; GOLDAMMER, J. G. (eds.). **Fire in the Environment**: the ecological, atmospheric, and climatic importance of vegetation fires. Chichester, England: J. Wiley & Sons,1993. p. 15-37.LONGO, K.; FREITAS, S.; ANDREAE, M. Biomass burning in Amazonia: emissions, long-range transport of smoke and its regional and remote impacts. In: KELLER, M.; BUSTAMANTE, M.; GASH, J.; SILVA DIAS, P. (eds.). **Amazonia and Global Change.** Washington, D. C: American Geophysical Union, 2009.,doi: 10.1029/2008GM000717.

LONGO, K. M. et al. The coupled aerosol and tracer transport model to the brazilian developments on the regional atmospheric modeling system (catt-brams)-part 2: Model sensitivity to the biomass burning inventories. **Atmospheric Chemistry and Physics**, v. 10, n. 13, p. 5785–5795, 2010.

LONGO, K. M. et al. The Chemistry CATT-BRAMS model (CCATT-BRAMS 4.5): a regional atmospheric model system for integrated air quality and weather forecasting and research. **Geoscientific Model Development**, v. 6, n. 5, p. 1389–1405, 9 set. 2013.

MARENCO, F. et al. On the vertical distribution of smoke in the Amazonian atmosphere during the dry season. **Atmospheric Chemistry and Physics**, v. 16, n. 4, p. 2155–2174, 12 nov. 2016.

MATSON, M.; DOZIER, J. Identification of subresolution high temperature sources using a thermal IR sensor. **Photogrammetric Engineering and Remote Sending,** v. 47, n. 9, p. 1311 - 1318, Sept., 1981.

MCCARTER, R.; BROIDO, A. Radiative and convective energy from wood crib fires. **Pyrodynamics**, v. 2, p. 62 - 85, 1965.

MONKS, P. S. et al. Tropospheric ozone and its precursors from the urban to the global scale from air quality to short-lived climate forcer. **Atmospheric**

Chemistry and Physics Discussions, v. 14, p. 32709–32933, 2014.

MOREIRA, D.; FREITAS, S.; BONATTI, J. Coupling between the JULES land-surface scheme and the CCATT-BRAMS atmospheric chemistry model (JULES-CCATT-BRAMS1. 0): applications to numerical. **Geoscientific Model Development,** v. 6, n. 4, p. 1243-1259, 2013. doi: <10.5194/gmd-6-1243-2013**>**.

MORGAN, W. et al. Overview of the South American biomass burning analysis (SAMBBA) field experiment. In: AIP CONFERENCE, 19., 2013, Vienna, Austria. **Proceedings…** AIP Publishing LLC, 2013.

OGURA, Y.; TAKAHASHI, T. Numerical simulation of the life cycle of a thunderstorm cell. **Monthly Weather Review**, v. 99, p. 895-911, 1971. http://dx.doi.org/10.1175/1520-0493(1971)0992.3.CO;2.

PAUGAM, R. et al. A review of approaches to estimate wildfire plume injection height within large scale atmospheric chemical transport models – Part 1. **Atmospheric Chemistry and Physics Discussions**, v. 15, n. 6, p. 9767–9813, 31 mar. 2015a.

PAUGAM, R. et al. Development and optimization of a wildfire plume rise model based on remote sensing data inputs – Part 2. **Atmospheric Chemistry and Physics Discussions**, v. 15, n. 6, p. 9815–9895, 31 mar. 2015b.

PEREIRA, G. et al. Estimating trace gas and aerosol emissions over South America: Relationship between fire radiative energy released and aerosol optical depth observations. **Atmospheric Environment**, v. 43, n. 40, p. 6388–6397, 2009.

PEREIRA, M. C. **Detecção, monitoramento e análises de alguns impactos ambientais de queimadas na Amazônia usando dados de avião e dos satélites NOAA e LANDSAT**. São José dos Campos: Instituto Nacional de Pesquisas Espaciais, 1988. (Não publicado)

PFISTER, G.; AVISE, J.; WIEDINMYER, C. CO source contribution analysis for

California during ARCTAS-CARB. **Atmospheric Chemistry and Physcs,** v**.**11, p. 7515-7532, 2011.

PICKERING, K.; DICKERSON, R. Trace gas transport in the vicinity of frontal convective clouds. **Journal of Geophysical Research,** v. 93, n. D1, p.759–773, 20 Jan. , 1988.

PRINS, E.; FELTZ, J.; MENZEL, W. An overview of GOES-8 diurnal fire and smoke results for SCAR-B and 1995 fire season in South America. **Journal of Geophysical Research,** v. 103, n. D24, p. 31,821-31,835, Dec. 27, 1998.

PRINS, E.; MENZEL, W. Geostationary satellite detection of bio mass burning in South America. **International Journal of Remote Sensing**, v. 37, n. 19, 1992.

PRINS, E.; MENZEL, W.; WARD, D. GOES-8 ABBA diurnal fire monitoring during SCAR-B. In: SMOKE/SULFATE, CLOUDS AND RADIATION–BRAZIL, 1996, Fortaleza. **Proceedings…** São José dos Campos: Transtec Editorial,1996.

PROCOPIO, A.; REMER, L.; ARTAXO, P. Modeled spectral optical properties for smoke aerosols in Amazonia. **Geophysical Research Letters**, v. 30, n. 24, 2003. doi:10.1029/2003GL018063.

REID, J. S. et al. Physical, chemical, and optical properties of regional hazes dominated by smoke in Brazil. **Journal of Geophysical Research**, v. 103, n. D24, p. 32059, 1 dez. 1998.

REMER, L. A. et al. The MODIS aerosol algorithm, products, and validation. **Journal of the Atmospheric Sciences**. v. 73, n. 9, http://dx.doi.org/10.1175/JAS3385.1, 2005.

RÉMY, S. et al. Two global climatologies of daily fire emission injection heights since 2003. **Atmospheric Chemistry and Physics Discussions**, v. 0, p. 1–42, 13 abr. 2016. doi:10.5194/acp-2015-1048.

RIGGAN, P. J. et al. Remote Measurement of Energy and Carbon Flux from Wildfires in Brazil. **Ecological applications**, v. 14, n. 3, p. 855–872, 2004.

ROSÁRIO, N. E. et al. Modeling the South American regional smoke plume: Aerosol optical depth variability and surface shortwave flux perturbation. **Atmospheric Chemistry and Physics**, v. 13, n. 6, p. 2923–2938, 2013.

ROSENFELD, D. TRMM observed first direct evidence of smoke from forest fires inhibiting rainfall. **Geophysical Research Letters**, v. 26, n. 20, p. 3105–3108, 15 out. 1999.

ROSSATO, L.; ALVALÁ, R. S.; TOMASELLA, J. Climatologia da umidade do solo no Brasil. In: CONGRESSO BRASILEIRO DE METEOROLOGIA, 12., 2002, Foz do Iguaçu. **Anais…** Rio de Janeiro: SBMet, 2002. p. 1910–1915.

SESSIONS, W. R. et al. An investigation of methods for injecting emissions from boreal wildfires using WRF-Chem during ARCTAS. **Atmospheric Chemistry and Physics**, v. 11, n. 12, p. 5719–5744, 2011.

SESTINI, M.; REIMER, E.; VALERIANO, D. Mapa de cobertura da terra da Amazônia legal para uso em modelos meteorológicos. In: In: SIMPÓSIO BRASILEIRO DE SENSORIAMENTO REMOTO, 11. (SBSR) 2003, Belo Horizonte. **Anais...** São José dos Campos: INPE, 2003. p. 2901 - 2906. CD-ROM. ISBN 85-17-00017-X. (INPE-16175-PRE/10778). Disponível em:<http://urlib.net/ltid.inpe.br/sbsr/2002/11.22.20.34>. Acesso em: 11 ago. 2016.

SETZER, A.; PEREIRA, M. Amazonia biomass burnings in 1987 and an estimate of their tropospheric emissions. **Ambio**. Stockholm, v. 20, p. 19 - 22, 1991.

SIMPSON, J.; WIGGERT, V. Models of precipitating cumulus towers. **Monthly Weather Review**, v. 97, n. 7, p. 471, 1969.

SOFIEV, M.; ERMAKOVA, T.; VANKEVICH, R. Evaluation of the smoke-injection height from wild-land fires using remote-sensing data. **Atmospheric**

Chemistry and Physics, v. 12, n. 4, p. 1995–2006, 21 fev. 2012.

THOMPSON, A.; PICKERING, K. Convective transport over the central United States and its role in regional CO and ozone budgets. **Journal of Geophysical Research**, v. 99, n. D9, 20 Sept. 1994, p. 18703–18711, 1994.

TOON, O.; TURCO, R.; WESTPHAL, D. A multidimensional model for aerosols: Description of computational analogs. **Journal of the Atmospheric Sciences,** v. 45, n. 15, p. 2123 - 2143, 1988.

TRIPOLI, G. The Colorado State University three-dimensional cloud/mesoscale model-1982 Part I: General theoretical framework and sensitivity experiments. **Journal de Recherches Atmospheriques,** v.16, n. 4, p. 295-320, Jan. 1982.

TURNER, J. **Buoyancy effects in fluids**. Cambridge: University Press.,, 1979.

VAL MARTIN, M. et al. Space-based observational constraints for 1-D fire smoke plume-rise models. **Journal of Geophysical Research: Atmospheres**, v. 117, n. 22, p. 1–63, 2012.

WALKO, R. et al. Coupled atmosphere-biophysics-hydrology models for environmental modeling. **Journal of applied Meteorology,**v. 39, p. 931 -944, 2000.

WARD, D.; SUSOTT, R.; KAUFFMAN, J. Smoke and fire characteristics for cerrado and deforestation burns in Brazil: BASE-B experiment. **Journal of …**, 1992.

WESELY, M. Parameterization of surface resistances to gaseous dry deposition in regional-scale numerical models. **Atmospheric Environment (1967)**, v. 23, n. 6**,** p. 1293-1304, 1989.

WOOSTER, M. J. et al. Retrieval of biomass combustion rates and totals from fire radiative power observations: FRP derivation and calibration relationships between biomass consumption and fire radiative energy release. **Journal of Geophysical Research**, v. 110, n. D24, p. D24311, 2005.